Partitioning of carbon export in the upper water column of the oligotrophic South China Sea

Yifan Ma[1], Kuanbo Zhou[1]. Weifang Chen[1], Junhui Chen[1], Jin-Yu Terence Yang[1] & Minhan Dai[1]

[1]State Key Laboratory of Marine Environmental Science, College of Ocean and Earth Sciences, Xiamen University, Xiamen, 361102, China

Correspondence to: Minhan Dai (mdai@xmu.edu.cn)

Abstract. We conducted ~~high vertical resolution~~ samplings of total and particulate ^{234}Th along with particulate organic carbon (POC) in the summer of 2017 to examine nutrient-dependent structures of export productivity within the euphotic zone (Ez) of the oligotrophic basin of the South China Sea (SCS). Nitrate concentrations throughout the study area were below detection limits in the nutrient-depleted layer (NDL) above the nutricline, while they sharply increased with depth in the nutrient-replete layer (NRL) across the nutricline until the base of the Ez. Based on our ~~high resolution~~ vertical profilings of ^{234}Th/^{238}U disequilibria, this study for the first time estimated POC export fluxes both out of the NDL and at the horizon of the Ez base. Total ^{234}Th deficit relative to ^{238}U occurred in the NDL at all study sites, while ^{234}Th was mostly in equilibrium with ^{238}U in the NRL except at the northmost station SEATS (116° E, 18° N), where the ^{234}Th deficit could also be observed in the NRL. By combining 1D ~~steady-state~~steady state ^{234}Th fluxes and POC/^{234}Th ratios, we derived vertical patterns of POC export fluxes. Values were 1.6±0.6 mmol C m^{-2} d^{-1} at the NDL base, representing approximately half of the flux estimated at the base of the Ez at station SEATS; for the rest of the sampling sites, POC export fluxes at the NDL base (averaged at 2.3±1.1 mmol C m^{-2} d^{-1}) were identical within error to those at the base of the Ez (1.9±0.5 mmol C m^{-2} d^{-1}), suggesting rapid export of POC out of the NDL. This finding fundamentally changes our traditional view that the NDL, being depleted in nutrients, would not be a net exporter of POC. Based on the positive relationship between POC export fluxes at the NDL base and supply potential of subsurface nutrients (i.e., nutricline depth and nutrient concentrations), we found that POC export fluxes (averaged 3.4±1.2 mmol C m^{-2} d^{-1}) at the NDL base at stations with shallow nutriclines and high subsurface nutrient concentrations were ~100% higher than the fluxes (averaged 1.6±0.5 mmol C m^{-2} d^{-1}) at other stations. We used a two-endmember mixing model based on the mass and ^{15}N-isotopic balances to further evaluate the potential sources of new nitrogen that could support the observed particle export at stations SEATS and SS1, located respectively in the northern and southern basin of the SCS with different hydrological features. We showed that more than 50% of the particle flux out of the NDL was supported by nitrate sources likely supplied from depth associated with episodic intrusions, other than atmospheric deposition and nitrogen fixation~~: likely supply from depth associated with episodic intrusions~~. However, the exact mechanisms and pathways for subsurface nutrients to support the export production from the NDL merit additional careful and dedicated studies.

Keywords: Export productivity, nutrient-depleted layer, ^{234}Th/^{238}U disequilibrium, the South China Sea

1 Introduction

The marine biological carbon pump (BCP) plays a central role in sequestrating atmospheric CO_2, thereby mitigating human-induced climate change. Despite great efforts that have been devoted to studying the BCP, there remain critical knowledge gaps in its structure, function and efficiency (Siegel et al., ~~2020~~2021). Recently, the EXPORTS (EXport Processes in the Ocean from RemoTe Sensing) program has implemented comprehensive experiments which examine export flux pathways, plankton community composition, food web processes, and biogeochemical properties of the ecosystem, to achieve an improved understanding of export fluxes and the BCP (Siegel et al., 2016; ~~2020~~2021).

Among other factors, depth-dependent particle export at different horizons within the euphotic zone (Ez), and how these exports are sustained by different nutrient sources, remains largely unknown. Most previous studies have treated the Ez as a single box and chose a fixed depth (e.g., 100 or 150 m) as the export horizon (Benitez-Nelson et al., 2001; Cai et al., 2015; Zhou et al., 2020a). A recent study has suggested that using a fixed depth instead of the *in situ* Ez depth as the export horizon would lead to the magnitude of global POC export flux being underestimated by a factor of two (Buesseler et al., 2020a). In the oligotrophic oceans, permanent stratification limits nutrient supply from depth; the Ez thus could be divided into a two-layer structure based on nutrient concentrations: (1) Nutrient-depleted Layer (NDL) between the ocean surface and the top of the nutricline, and (2) Nutrient-replete Layer (NRL) between the nutricline and the base of the Ez (Du et al., 2017). Conventional concepts suggest that regenerated nutrients predominantly support biological productivity in the NDL where export production is limited due to the absence of new nutrient supplies (Eppley and Peterson, 1979; Goldman, 1984). Meanwhile, Coale and Bruland (1987) noticed layer~~r~~ed structure of ^{234}Th-^{238}U disequilibria in the Ez, composed of an upper oligotrophic layer characterized by low new production values, low net scavenging; and a subsurface eutrophic layer with higher new production values, and suggested that new production rather than total primary production determined the scavenging of the reactive elements such as ^{234}Th.

Along with the increasing attention on BCP in the oligotrophic ecosystems~~Recently~~, some observations have however indicated that particles sourced from surface waters with extremely low nutrient concentrations may substantially contribute to the downward fluxes at depth. Scharek et al. (1999) observed that the diatom-diazotroph assemblages (*H.hauckii* contained *Richelia*-type endosymbionts with heterocysts) in the surface nutrient-deficient mixed layer dominated downward particle fluxes collected by a sediment trap at 150 m depth at the oligotrophic station ALOHA (158° W, 22° N). Liu et al. (2007) observed consistent $\delta^{13}C_{POC}$ values between sediment trap samples collected at 100 m and suspended particles in the upper 20 m in the South China Sea (SCS) basin, likely suggesting that the trapped particles were predominantly originated from the surface (i.e., 20 m). The ecosystem in nutrient-depleted surface waters may therefore play an important role in carbon export. Different pathways to introduce new nutrients have been suggested to support the carbon export from the NDL; for example, high rates of nitrogen fixation in the NDL could support 26-47% of the particle fluxes at station ALOHA (Böttjer et al., 2017). In addition, episodic eddy events that uplift the nutricline and deliver deep stocks of nutrients to the NDL might also contribute

to POC export from the upper ocean (Johnson et al., 2010). Nevertheless, it remains unclear how the different nutrient supply to the surface waters affects the downward POC export flux at the NDL and Ez horizons.

The semi-enclosed South China Sea (SCS), the largest marginal sea in the North Pacific Ocean, is characterized by an oligotrophic basin due to intensive stratification (Du et al., 2017). Several previous studies quantified the ^{234}Th-based POC export flux and explored the mechanisms controlling export in the SCS. Seasonally, POC export fluxes are elevated in winter driven by the deepening of the mixed layer and nutrient supply from depth (Zhou et al., 2020a). Spatially, Cai et al. (2015) found that POC export fluxes decreased with distance offshore in the northern SCS due to reduced POC stocks. Mesoscale processes can also promote POC export by pumping nutrient-replete waters from depth into the Ez (Zhou et al., 2013; 2020b). Regardless, POC export fluxes at different export horizons, and the sources of new nutrients that support export, remain understudied in the oligotrophic SCS.

In this study, we conducted samplings of ^{234}Th at a reasonably high depth resolution in the Ez during the summer of 2017 to examine the structure of export productivity partitioning in the SCS basin. We calculated POC export fluxes based on ^{234}Th from both the NDL and Ez. Based on trap-derived masses and ^{15}N-isotopic balances, we estimated the relative contributions of different nutrient sources to export fluxes within the two-layer nutrient-based structure in the SCS at two stations with different hydrological features. Moreover, we related POC export fluxes from the two layers to their different biogeochemical forcings (especially the depth of the nutricline and the subsurface nutrient concentrations), to examine the controlling factors that potentially regulate POC export flux in the oligotrophic SCS.

2 Methods

2.1 Sample collection

Ship-based sampling was conducted from June 5th to 27th, 2017 on the R/V Tan Kah Kee in the SCS basin (Fig. 1 and Table 1) under the umbrella of the CHOICE-C II project (**Carbon cycle in the South China Sea: budget, controls and global implications**). We visited two mega stations (SEATS and SS1) and 9 regular stations during the cruise. The *in situ* observation at Station SEATS was conducted before a typhoon (Merbok) which potentially affected the biogeochemistry of the region, and the remaining stations were visited after the typhoon (listed in Table 1). To examine the spatial variability of ^{234}Th, we sampled four closely-clustered stations (H01, H06, H08, and H11) around Station SS1. Seawater samples were collected using 12-L or 10-L Niskin bottles attached to a Seabird 911 conductivity-temperature-depth (CTD) profiler.

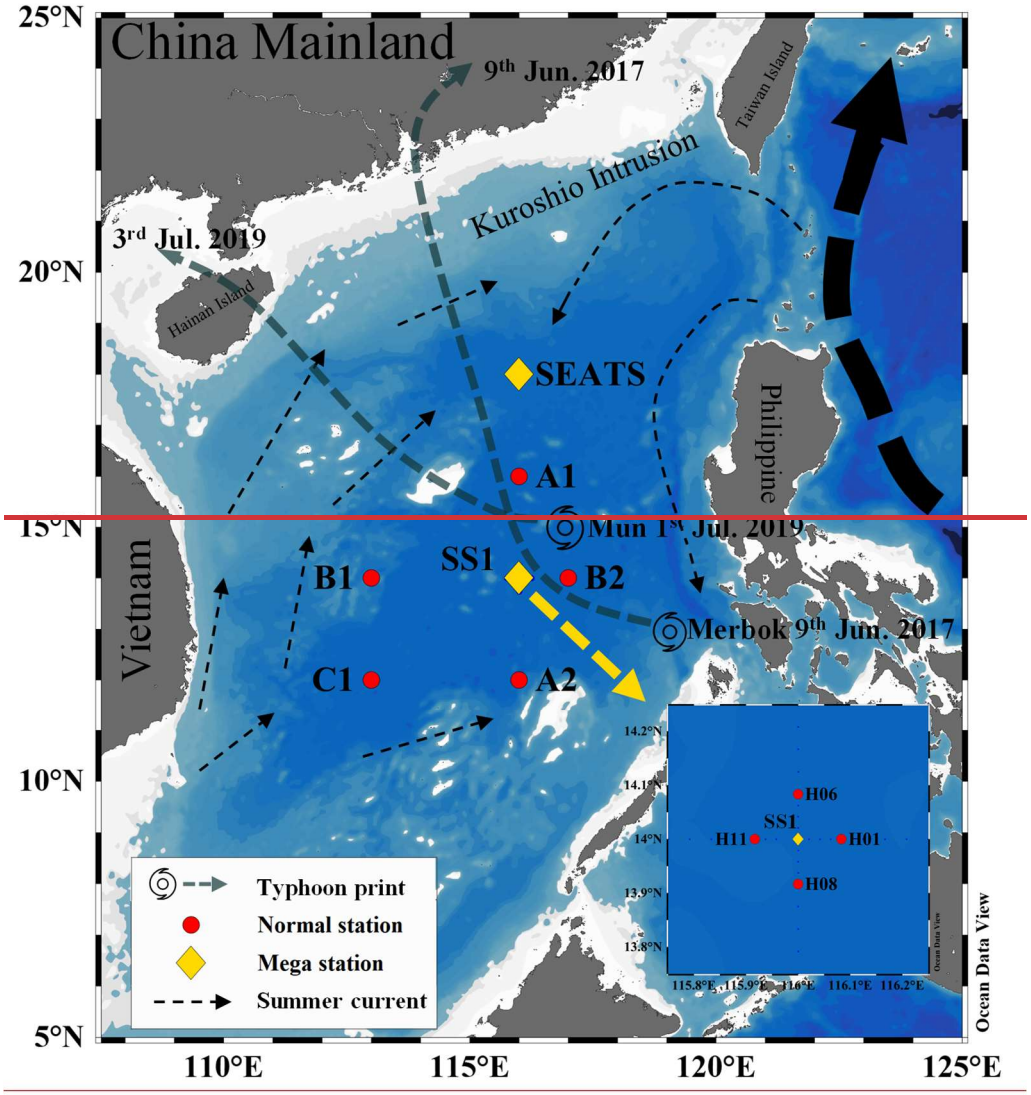
China Mainland
9th Jun. 2017
Taiwan Island
Kuroshio Intrusion
3rd Jul. 2019
Hainan Island
SEATS
Philippine
A1
Mun 1st Jul. 2019
SS1
B1
B2
Merbok 9th Jun. 2017
Vietnam
C1
A2
H06
H11
SS1
H01
H08
Typhoon print
Normal station
Mega station
Summer current
Ocean Data View
25°N
20°N
15°N
10°N
5°N
110°E
115°E
120°E
125°E

95

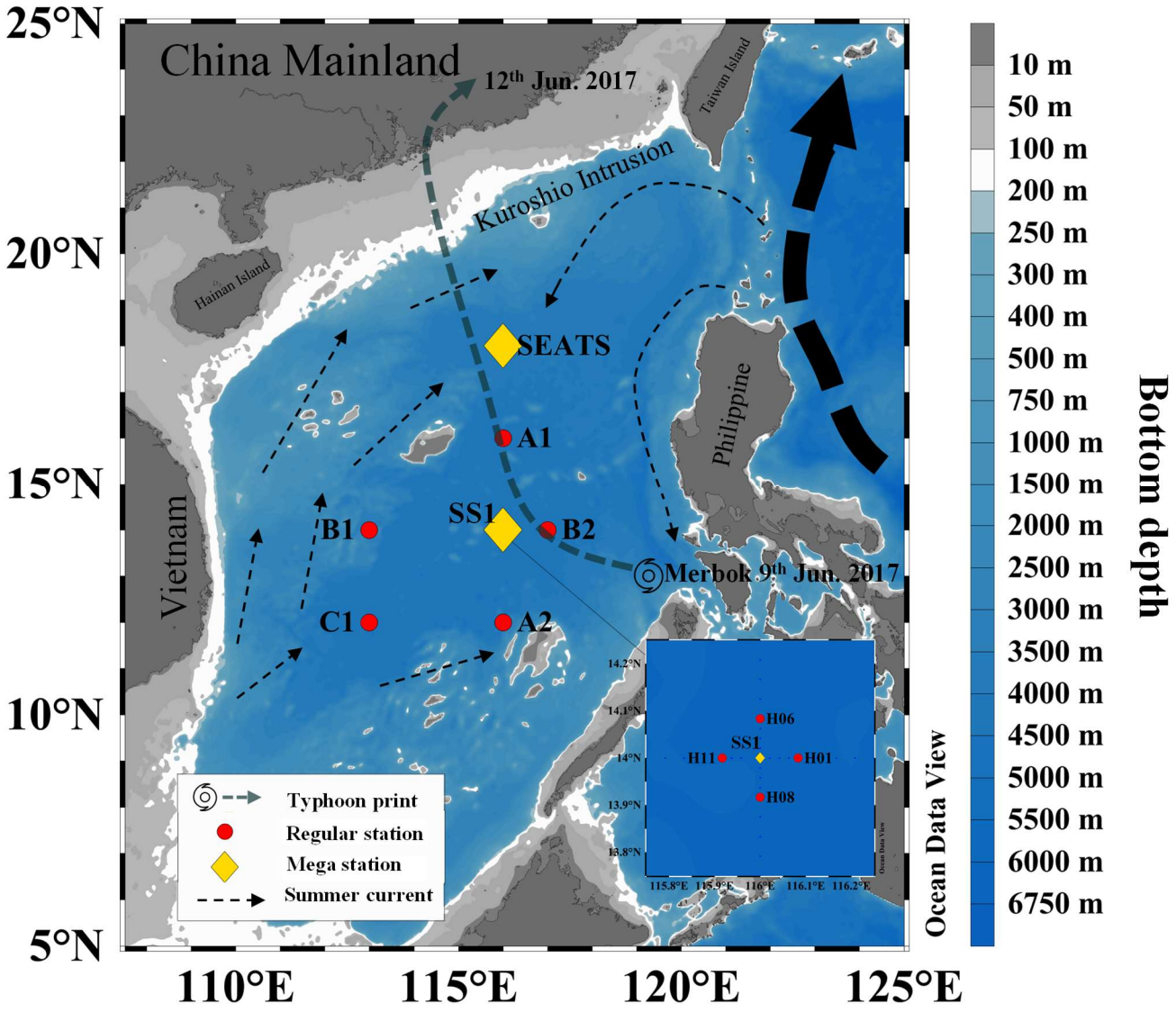

Figure 1: Map of the South China Sea (SCS) with sampling stations during June 2017. Yellow diamonds denote mega stations (SEATS and SS1) where high-resolution sampling was conducted at a 10-m interval in the euphotic zone; red circles denote regular stations where samples were collected at typical sampling depths of 5, 25, 50, 75 and 100 m. The general circulation pattern (adapted from Liu et al., 2016) is also shown. The dominant summer currents are denoted by black dashed arrows. The dark blue dashed line denotes the path of typhoon Merbok (generated at the southeastern part of the SCS on June 9th, 2017).

Table 1: Sampling logs and site information along with the accessed parameters and their utilizations.

Station	Arriving time	Latitude [°N]	Longitude [°E]	Bottom depth [m]	Parameters		Data utilizations	
					Total ^{234}Th	Trap	Partitioning POC flux estimate	Nutrient source diagnosis
SEATS	2017-06-07 00:06	18.0	116.0	3907	√	√	√	√
A1*	2017-06-11 23:55	16.0	116.0	4205	√		√	
SS1	2017-06-12 20:08	14.0	116.0	4107	√		√	
H06	2017-06-20 02:28	14.1	116.0	4289	√		√	
H08	2017-06-20 07:51	13.9	116.0	4063	√		√	
H01	2017-06-20 23:41	14.0	116.1	4139	√		√	
H11	2017-06-21 05:18	14.0	115.9	4297	√		√	
B1	2017-06-22 11:43	14.0	113.0	2537	√		√	
C1	2017-06-23 04:40	12.0	113.0	4313	√		√	
A2	2017-06-24 03:05	12.0	116.0	4079	√		√	
B2	2017-06-24 21:42	14.0	117.0	3947	√		√	

*Sampling station might be influenced by the typhoon event passing through the South China Sea. Station A1 was visited right after typhoon Merbok, which was generated on June 9th, 2017 at 13.1°N, 119.8°E in the southern South China Sea. Merbok landed on June 12th at 27.5°N, 117.3°E.

At the mega stations, high vertical resolution water samples were taken at a depth interval of 10 m within the Ez. For regular stations, lower resolution (5, 25, 50, 75 and 100 m) samples were collected. 4 L and 8 L seawater volumes were collected for

total ^{234}Th and particulate ^{234}Th/POC analysis, respectively. Samples were collected using acid clean 4-L fluorinated bottles and filtered onto quartz microfiber (QMA) filters (25 mm diameter, 1.0 μm pore size). 500-mL of seawater was also collected for nutrient analysis from the Niskin bottles. Ancillary parameters, including potential temperature, salinity and fluorescence, were accessed using a seabird CTD sensor. We calibrated the sensor-derived fluorescence with the Chl *a* concentrations from discrete samples using the equation: Chl *a* (mg m^{-3}) = 0.855×fluorescence (R^2 =0.87, n=139, Fig. S1).

In addition, we deployed an array of floating sediment traps for 72 hours at 50, 100 and 200 m at both mega stations SEATS and SS1 to collect sinking particles during the survey. Retrieval of the trap at Station SS1 was precluded by unfavorable sea conditions. Consequently, we utilized sediment trap data acquired during a 53-hour deployment in July 2019. Our choice of alternative data collection is unlikely to engender bias in our analysis, as evidenced by the limited interannual variability in ^{15}N signals of sinking particles obtained from sediment traps (see details in Section 3.5). At each depth of stations SEATS and SS1, 12 cylindrical acrylic tubes (with a height of 50 cm and diameter of 10 cm) were assembled for different biogeochemical measurements. Before deployment, the tubes were filled with prefiltered surface seawater and NaCl was added to supersaturation. After recovery, the tubes were placed under 4°C until the particles settled to the bottom. After removing the overlying supernatant, the particles were prefiltered through Nitex filters (120 μm pore size) to remove the visible zooplankton and then collected on QMA filters (1.0 μm pore size) for elemental and isotopic analyses.

2.2 ^{234}Th analysis

The small-volume (4 L) MnO_2 co-precipitation method was used for the total ^{234}Th analysis (Benitez-Nelson et al., 2001; Cai et al., 2006). The efficiency of thorium precipitation was monitored by ^{230}Th. In detail, the seawater samples were acidified after collection and spiked with 200 μL of ^{230}Th (17.38 dpm mL^{-1}). After an 8-hour period to allow equilibration between samples and tracers, the pH of seawater was raised to 8.05-8.20 using $NH_3 \cdot H_2O$ before 0.375 ml $KMnO_4$ (3.0 g L^{-1}) and 0.20 ml $MnCl_2$ (8.0 g L^{-1}) were added. The MnO_2 precipitates were collected for a total ^{234}Th and the particles filtered for particulate ^{234}Th from the seawater samples on a QMA filter (25 mm, 1.0 μm) were dried in the oven overnight under 45°C. The filters were then packed with Teflon rings and discs (diameter of 23.5 cm, produced by RISØ National Laboratory, Denmark) covered by Al foil (density: 6.45 mg m^{-2}) and Mylar film. A gas-flow proportional low-level RISØ beta counter (Model GM-25-5) was used for ^{234}Th counting. The first count was carried out immediately after the samples were set up, and the second count was carried out after > 6 months for the background measurement. All ^{234}Th samples were counted for 1000 minutes each time. The ^{230}Th was monitored using ^{229}Th, which was purified after iron precipitation and anion column exchange, and the concentrated was finally diluted to 6 mL in 2% HNO_3. The samples were then settled into 15-ml centrifuge tubes and measured by inductively coupled plasma-mass spectrometry (ICP-MS) (Agilent 7700x). The average of all the recoveries was 88±12 % (mean±1σ, n = 97, range 73-98%). All ^{234}Th data were recovery- and decay-corrected to the sampling time. The uncertainties of ^{234}Th data were propagated from the counting error, uncertainty from recovery and detection efficiency. The ^{238}U activity was estimated by the following equation assuming conservative behavior with respect to salinity (Owens et al., 2011):

$$^{238}U = 0.0786 \times S - 0.314\ , \quad (1)$$

2.3 POC, PN and $\delta^{15}N_{PN}$ analyses

Upon ^{234}Th counting, the particulate samples were carefully removed from the discs and placed in glass dishes. Subsequently, the filters were dried at 50 °C for 24 hours after adding 0.4 mL of HCl (1.0 μmol L^{-1}) to remove inorganic carbon. POC and particulate nitrogen (PN) concentrations were determined by an Elemental Analyzer-Isotope Ratio Mass Spectrometer (EA-IRMS) system~~POC and PN concentrations were determined by an Elemental Analyzer- Isotope Ratio Mass Spectrometer (EA-IRMS) system~~ (EA:vario PYRO cube and IRMS: Isoprime 100). At station SS1, we conducted 10 replicate POC samplings at 5, 100 and 200 m water depth to investigate the precision of bottle-collected POC. Our results show that the standard deviations of our analyses were better than 13%, which agrees well with the result from the JGOFS cookbook (Knap et al., 1996). The errors were included in the subsequent calculation of POC export fluxes. The particles from the sediment traps were treated the same as the suspended particles. The C and N contents and the isotopes of sinking particles were also analyzed by EA-IRMS.

2.6~~4~~ The depth of the euphotic zone

The euphotic zone depth (Zeu or the Ez base, in m) is defined optically, based on Wu et al. (2021), as the depth where the usable solar radiation (USR) equals 0.9% of the surface USR, which is close to the depth where the photosynthetically available radiation (PAR) equals 0.5% of the PAR value at the sea surface. *In-situ* Zeu during the cruise was obtained from profiling PAR data recorded by the optical sensor (Biospherical QCP2300-HP) on the CTD.

2.7~~5~~ Nutrient analysis and nutricline depth

Nutrients were analysed onboard using a Four-channel Continuous Flow Technicon AA3 Auto-Analyzer (Bran-Lube GmbH). The detection limits for both N+N (nitrate plus nitrite, termed as dissolved inorganic nitrogen, DIN) and dissolved inorganic phosphorus (DIP)~~SRP (soluble reactive phosphate)~~ were 0.03 μmol L^{-1}. The top of the nutricline in this study was defined as the depth at which the DIN concentration reached 0.1 μmol L^{-1} (Dore and Karl, 1996; Winn et al., 1996). The layers above, and below to the base of Ez, were defined as the as NDL and NRL, respectively.

2.~~4~~ 6 ^{234}Th scavenging model

The mass balance for ^{234}Th in seawater can be described as Eq. (2) (Buesseler et al., 1992):

$$\frac{\partial A_{Th}^{total}}{\partial t} = \lambda\left(A_U - \partial A_{Th}^{total}\right) - F_{Th} + V \quad \frac{\partial A_{Th}^{total}}{\partial t} - \lambda(A_U - A_{Th}^{total}) - F_{Th}^{j} + F_{Th}^{j-1} + V\ , \quad (2)$$

where F_{Th} is the ^{234}Th scavenging flux ~~in the layer *i*, and F_{Th}^{i-1} is the ^{234}Th scavenging flux above the layer *i*. We assume F_{Th}^{i-1} = 0 when we calculate ^{234}Th flux for the initial layer (*i* = 1)~~at the export horizon. A_U and A_{Th}^{total} are the ^{238}U and total ^{234}Th activities, and λ is the ^{234}Th decay constant (0.02876 d^{-1}); *V*, which is discussed below, is the term for physical effects, including advection and diffusion.

For particle export from the Ez, the deficit of total ^{234}Th relative to ^{238}U is integrated with depth to evaluate ^{234}Th fluxes. Under the assumption of steady state ~~(SS)~~ ($\frac{\partial A_{Th}^{total}}{\partial t} = 0$) and no physical transport ($V = 0$), the ^{234}Th export flux from the Ez (F_{Th}^{Ez}) is integrated by Eq. (3) (as shown in Fig. 2):

~~$\frac{\partial A_{Th}^{total}}{\partial t} = \lambda(A_U - A_{Th}^{total}) - F_{Th}^{i} + F_{Th}^{i-1} + V$,~~ $F_{Th}^{Ez} = \int_0^{Ez} (A_U - A_{Th}) \times \lambda dz$, (3)

Similarly, ^{234}Th export flux from the base of the NDL, F_{Th}^{NDL}, is estimated as follows:

$$F_{Th}^{NDL} = \int_0^{NDL} (A_U - A_{Th}) \times \lambda dz, \quad (4)$$

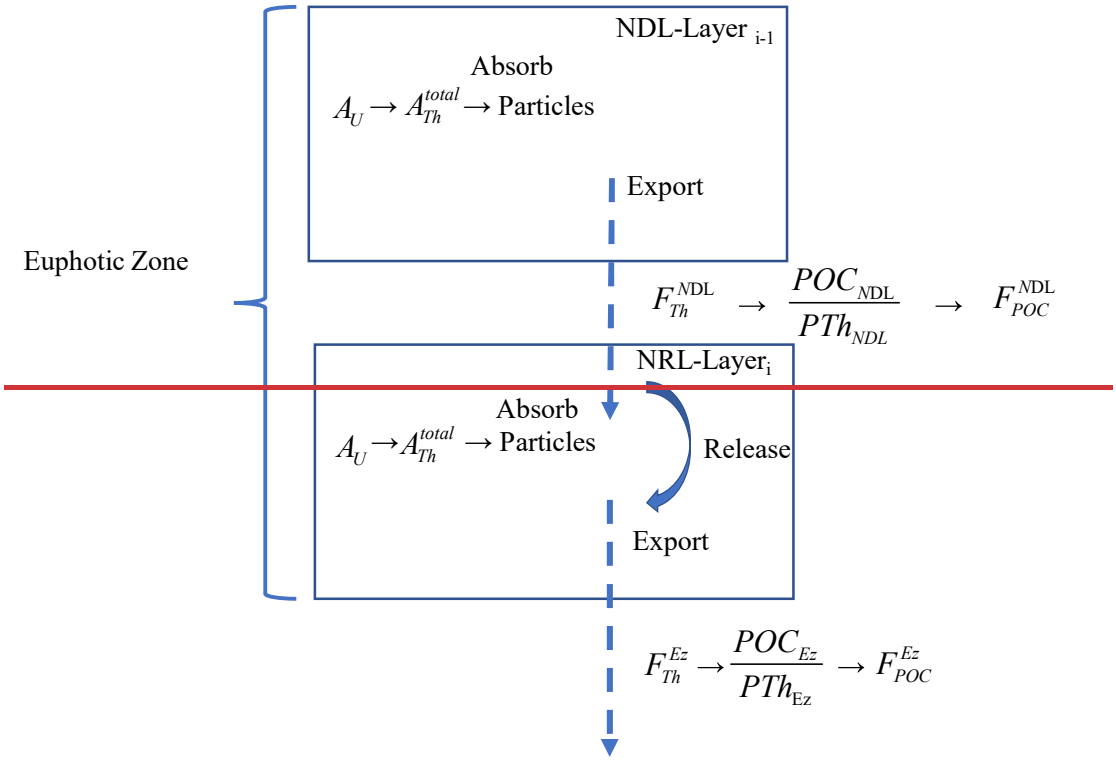

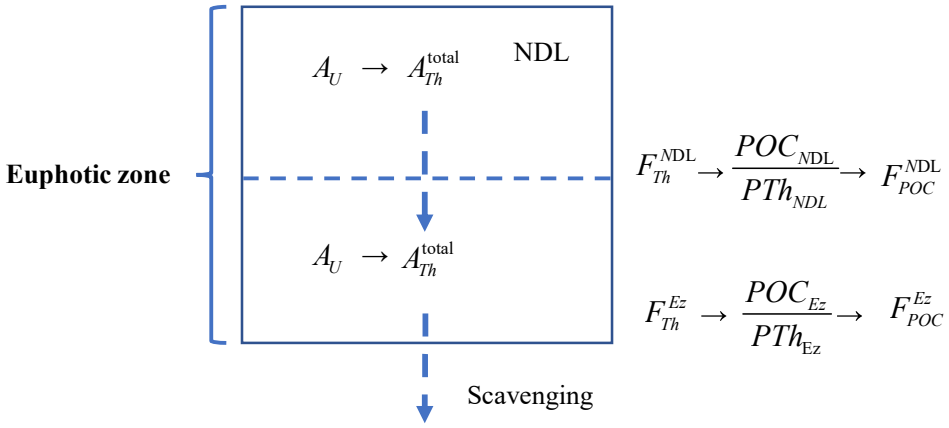

Figure 2: Schematic of the ^{234}Th model under the two-layer nutrient structure. All terms are defined in Eq. (2)-(4) and Eq. (7)-(9).

However, the assumption of no physical transport needs to be verified before ^{234}Th flux was calculated. In this study, the physical transport is estimated as follows:

$$V=-u\times\frac{\partial A_{Th}}{\partial x}-v\times\frac{\partial A_{Th}}{\partial y}-w\times\frac{\partial A_{Th}}{\partial z}+K_x\frac{\partial^2 A_{Th}}{\partial x^2}+K_y\frac{\partial^2 A_{Th}}{\partial y^2}+K_z\frac{\partial^2 A_{Th}}{\partial z^2}, \quad (5)$$

where u, v, and w are the zonal, meridional, and upwelling velocities respectively, $\frac{\partial A_{Th}}{\partial x}$, $\frac{\partial A_{Th}}{\partial y}$ and $\frac{\partial A_{Th}}{\partial z}$ are ^{234}Th activity gradients from west to east, south to north, and upward. K_x, K_y and K_z are diffusivities from west to east, south to north, and upward, respectively, and $\frac{\partial^2 A_{Th}}{\partial x^2}$, and $\frac{\partial^2 A_{Th}}{\partial z^2}$ are the second derivatives of ^{234}Th activity distributions (Benitez-Nelson et al., 2001; Cai et al., 2008; Buesseler et al., 2020b).

To better constrain the ^{234}Th flux in the SCS basin, we estimated the horizontal and vertical transports of ^{234}Th at the Station SS1. The climatological w and K_z from modeling results (Gan et al., 2016) were applied to the equation to evaluate the impacts of vertical advection and diffusion on the ^{234}Th flux. The vertical transport fluxes were -2.0±0.4 and -11.4±0.1 dpm m^{-2} d^{-1} at the bases of NDL and Ez, respectively, which can be considered negligible (less than 10%) compared to the vertical scavenging flux at the station SS1. This was in agreement with Cai et al. (2008) who also showed that the vertical term could be neglected for ^{234}Th flux estimation in the SCS basin.

The apparent diffusivity around station SS1 is estimated as ~4×10^5 cm^2 s^{-1} (Okubo, 1971) from empirically derived oceanic diffusion diagrams, and we simplified the horizontal diffusive term in Eq. (5) based on Benitez-Nelson et al. (2000) as follows:

$$V_{diffusion}=\sqrt{\frac{\left[K_x\left(A_{Th-H11}-2\times A_{Th-SS1}+A_{Th-H01}\right)\right]^2}{\Delta x^2}+\frac{\left[K_y\left(A_{Th-H08}-2\times A_{Th-SS1}+A_{Th-H06}\right)\right]^2}{\Delta y^2}}, \quad (6)$$

The Δx and Δy are the distance between the stations to evaluate the influences of physical terms (i.e., Δx is the distances between stations H01 and H11; Δy is the distances between stations H06 and H08). Δx and Δy were equal to 18 km in this study. Thus, the ^{234}Th flux derived from horizontal diffusion was considerably low (approximately 0.1 dpm m^{-2} d^{-1}).

The *in situ* horizontal current velocities at station SS1 from the Acoustic Doppler Current Profiler (ADCP) exhibited a wide range from 0.01 m s^{-1} to 0.3 m s^{-1} in the upper 200 m. Since these current velocities were measured instantaneously and their timescales did not match those of ^{234}Th (~ 20 days), we applied model-derived time-integrated data (three-month average) to the equation instead. The model-derived u and v ranged from 0.007 m s^{-1} to 0.2 m s^{-1} in the upper 100 m. Based on those velocities, the ^{234}Th flux from horizontal transport was about 15% of the ^{234}Th flux estimated using the steady state model in the upper 100 m, which is consistent with previous studies in oligotrophic ecosystems (e.g., Cai et al., 2008; Buesseler et al., 2020b). Thus, a 1D-model assumption is applicable in this study for the subsequent ^{234}Th flux estimation.

2.7 POC export flux calculation

In this study, the ^{234}Th-derived POC export flux was calculated using the following equations:

$$F_{POC}^{Ez} = F_{Th}^{Ez} \times \frac{POC_{Ez}}{PTh_{Ez}}, \quad (7)$$

where F_{Th}^{Ez}, $\frac{POC_{Ez}}{PTh_{Ez}}$ and F_{POC}^{Ez} are the ^{234}Th flux, particulate POC/^{234}Th ratio, and POC flux at the Ez base, respectively.

$$F_{POC}^{NDL} = F_{Th}^{NDL} \times \frac{POC_{NDL}}{PTh_{NDL}}, \quad (8)$$

where F_{Th}^{NDL}, $\frac{POC_{NDL}}{PTh_{NDL}}$ and F_{POC}^{NDL} are the ^{234}Th flux, particulate POC/^{234}Th ratio, and POC export flux at the NDL base, respectively.

Sediment trap-derived POC export fluxes were calculated as follows:

$$F_{POC-Trap} = \frac{POC_{Measured}}{\Delta t \times A_{Trap\,Tube}}, \quad (9)$$

where POC is the concentration of organic carbon on the particles collected by the traps, Δt is the duration of trap deployments, and $A_{TrapTube}$ is the area of the trap tube.

~~**2.6 The depth of the euphotic zone**~~

~~The euphotic zone depth (Zeu or the Ez base, in m) is defined optically, based on Wu et al. (2021), as the depth where the usable solar radiation (USR) equals 0.9% of the surface USR, which is close to the depth where the photosynthetic available~~

~~radiation (PAR) equals 0.5% of the PAR value at the sea surface. *In-situ* Zeu during the cruise was obtained from profiling PAR data recorded by the optical sensor (Biospherical QCP2300-HP) on the CTD.~~

~~2.7 Nutrient analysis and nutricline depth~~

~~Nutrients were analysed onboard using a Four-channel Continuous Flow Technicon AA3 Auto-Analyzer (Bran-Lube GmbH). The detection limits for both N+N (nitrate plus nitrite, termed as dissolved inorganic nitrogen, DIN) and SRP (soluble reactive phosphate) were 0.03 μmol L^{-1}. The top of the nutricline in this study was defined as the depth at which the DIN concentration reached 0.1 μmol L^{-1} (Dore and Karl, 1996; Winn et al., 1996). The layers above, and below to the base of Ez, were defined as the as NDL and NRL, respectively.~~

3 Results

3.1 Environmental settings

The profiles of ~~potential~~ temperature~~-~~ and salinity ~~(θ-S) diagram of the water column reveals~~ reveal distinctive hydrological features between stations in the SCS basin~~. The spatial differences in the hydrography were significant~~ (Fig. 3). The surface mixed layer depth (MLD, defined as the depth where the potential density σ_θ increased by 0.03 kg m^{-3} compared to the value at the sea surface, Cornec et al., 2021) at stations SEATS, A1, A2 and C1 was shallower (20-39 m) than at other stations ~~in the sampling region~~ (MDL>40 m, Table 2 and~~,~~ Fig. 3). The shallower MLD and isoclines (i.e., thermocline and halocline) might indicate upward displacement of waters at those stations. Du et al. (2021) attributed such vertical shifts in isoclines to mesoscale processes or basin scale circulation. Indeed, most of these stations (SEATS, A1 and C1) were under the influence of eddies during the sampling periods as revealed by the Sea level Anomaly (SLA) map (Fig. S2); modelling results indicate stations C1 and A2 were impacted by cold water sourced from the southwestern SCS basin derived from upwelling off the coast of Vietnam ~~when they were sampled~~ (Fig. S3) (Gan et al., 2016).

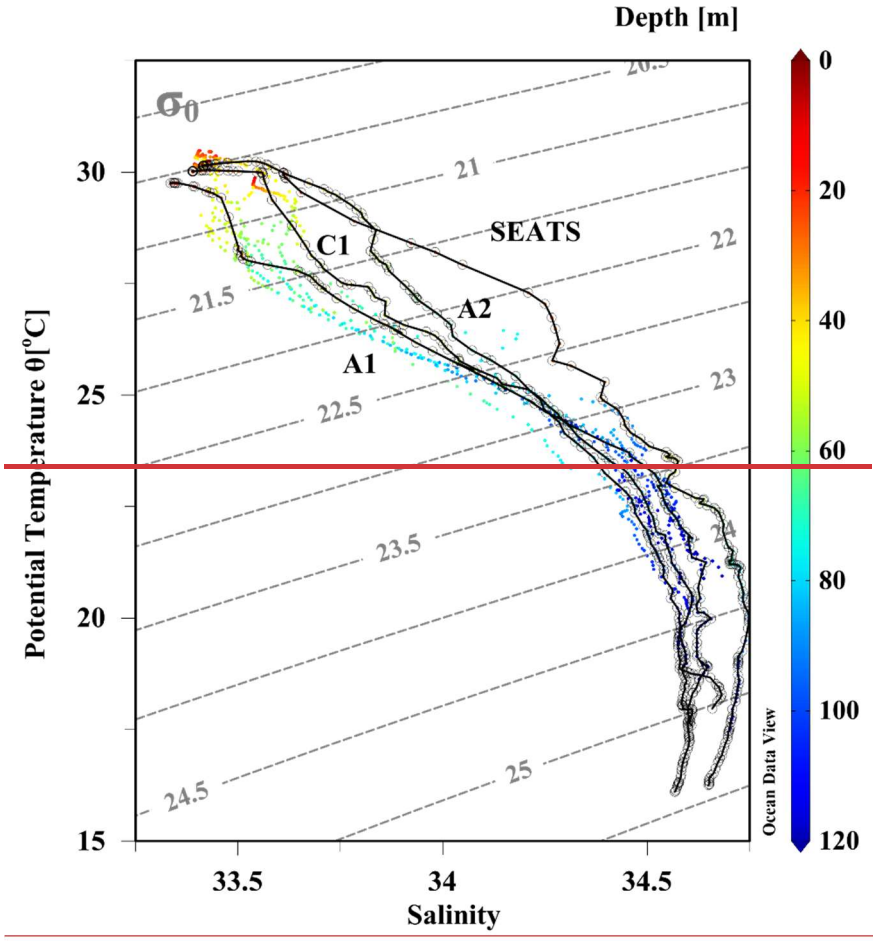

~~**Figure 3.** Plot of potential temperature (θ) vs. salinity (S) (θ-S diagram) for the sampling stations in the South China Sea basin during June 2017. Superimposed are sampling depths as shown in the color bar. The stations with shallow mixed layer depths (MLDs), i.e., stations SEATS, A2, C1 and A1, are highlighted with solid black lines.~~

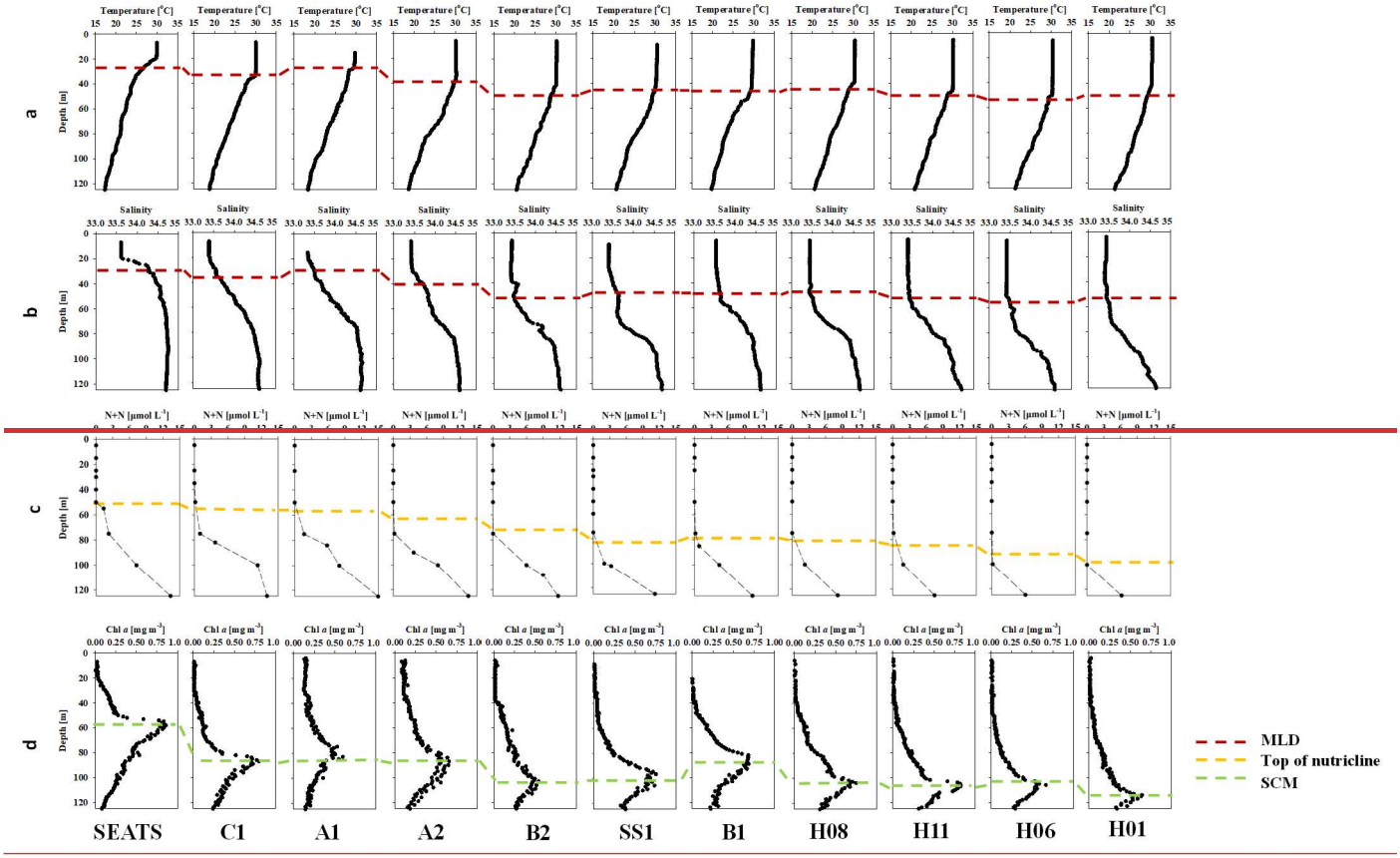
a
b
c
d
Temperature [°C]
Salinity
N+N [μmol L-1]
Chl a [μg m-3]
Depth [m]
MLD
Top of nutricline
SCM
SEATS
C1
A1
A2
B2
SS1
B1
H08
H11
H06
H01

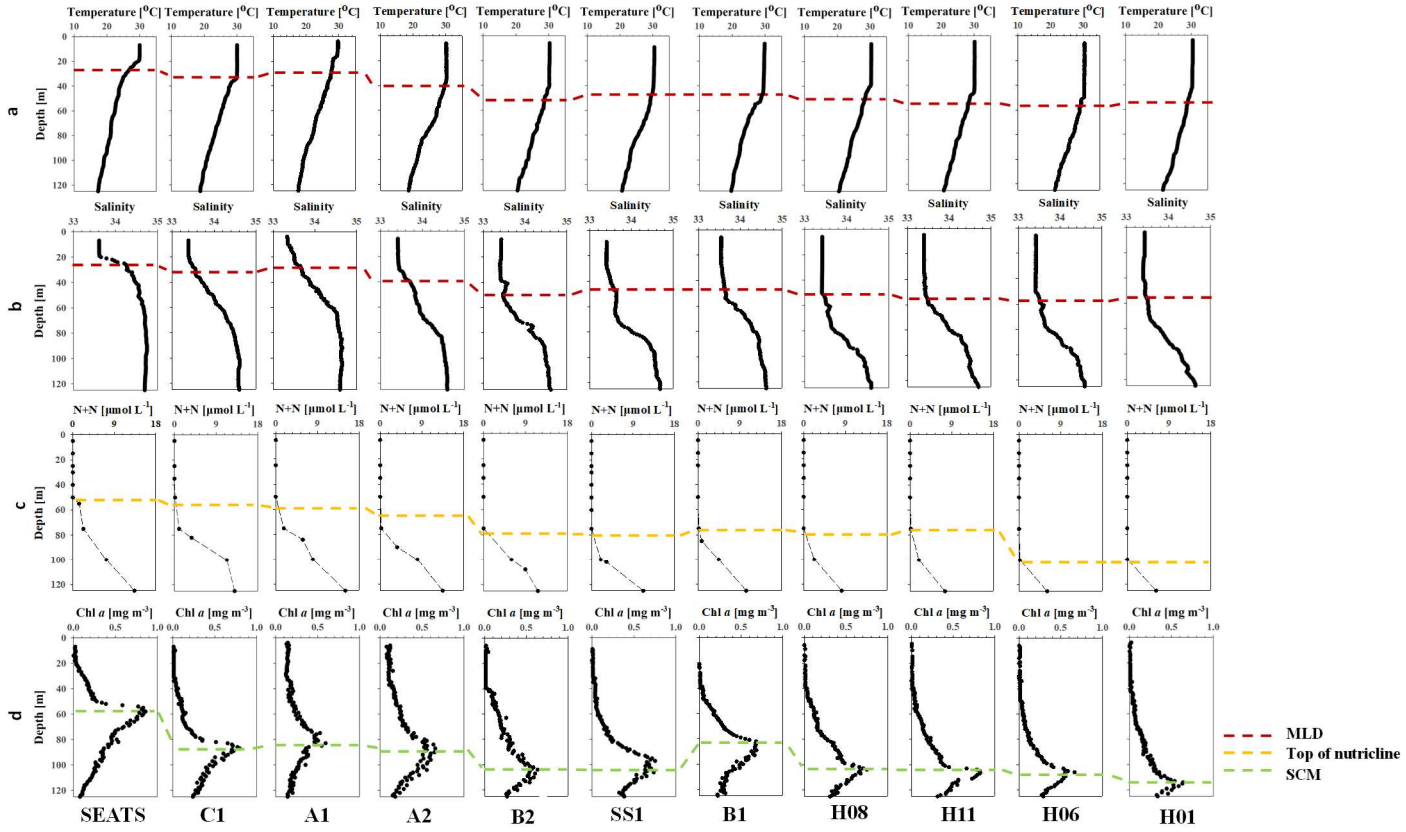

Figure 3: Vertical profiles of temperature (a), salinity (b), dissolved inorganic nitrogen (nitrate + nitrite, DIN, c) and Chl *a* (d). The MLD (red dash), interpolated depth of DIN=0.1 —µmol L^{-1} (top of nutricline, yellow dash) and subsurface Chl *a* Maximum (SCM, green dash) are also shown.

Table ~~1~~2: Surface mixed layer depths (MLDs), export horizon depths, 1D- steady state ^{234}Th fluxes, POC/^{234}Th ratios, and POC fluxes at stations in the upper oligotrophic South China Sea basin during June 2017

Station	[1]MLD	[2]NDL base	[3]Ez base	^{234}Th flux @ NDL	^{234}Th flux @ Ez	POC/^{234}Th ratio @NDL	POC/^{234}Th @Ez	POC export flux @ NDL	POC export flux @ Ez
	[m]	[m]	[m]	dpm m^{-2} d^{-1}	dpm m^{-2} d^{-1}	µmol C dpm^{-1}	µmol C dpm^{-1}	mmol C m^{-2} d^{-1}	mmol C m^{-2} d^{-1}
SEATS	27	50	80	362±34	522±43	4.4±0.6	5.5±0.7	1.6±0.6	2.9±0.7
C1	36	59	87	598±57	602±22	6.2±0.8	2.9±0.4	3.7±0.9	1.7±0.4
A1	27	57	88	603±98	585±100	7.1±0.9	5.2±0.7	4.3±1.2	3.0±0.8
A2	39	63	96	624±52	839±59	6.3±0.8	2.7±0.3	3.9±0.9	2.2±0.4
B2	44	71	102	204±57	267±69	8.2±1.1	8.3±1.1	1.7±1.2	2.2±1.2
SS1	43	81	111	613±42	631±48	4.0±0.5	3.1±0.4	2.4±0.5	2.0±0.4
B1	50	78	87	361±63	421±64	4.1±0.5	3.8±0.5	1.5±0.6	1.6±0.6
H08	42	80	106	376±61	462±68	5.8±0.8	4.6±0.6	2.2±0.8	2.1±0.7
H11	48	82	106	360±61	393±66	3.2±0.4	4.1±0.5	1.1±0.5	1.6±0.6
H06	52	87	115	439±63	462±66	3.2±0.4	2.8±0.4	1.4±0.5	1.3±0.4
H01	48	99	107	351±70	350±70	3.3±0.4	3.3±0.4	1.2±0.5	1.2±0.5

[1]The MLD ~~was~~ is defined as the depth where the potential density σ_θ ~~increased~~ increases by 0.03 kg m^{-3} compared to values at sea surface (Cornec et al., 2021).

[2]The NDL base, ~~namely~~ or the top of the nutricline, was interpolated to the depth where DIN = 0.1 µmol L^{-1} based on the DIN distribution near the SCM.

[3]The Ez base ~~was~~ is estimated to be the depth where PAR is 0.5% of the PAR value at the sea surface.

As shown in Fig.~~ure~~ 3c, nutrients were depleted in ~~the~~ surface waters until the top of the nutriclines where concentrations started to rapidly~~and~~ increase~~d with depth~~. ~~Nutrient~~ The depth profiles also show a clear relationship between ~~distinctive spatial pattern between the stations: shallower top of~~ nutricline~~s~~ and subsurface nutrient concentrations. ~~depths at 4~~The four stations (i.e., stations SEATS, C1, A1 and A2) with shallower nutriclines well correspond with higher subsurface nutrient concentrations. For example, DIN concentrations at 125 m in these four sites ~~at 125 m (Figure 3c) at those stations compared to others (DIN and dissolved inorganic phosphorus [DIP] concentrations at ~125 m~~ ranged from 13.1 ~~–~~to 17.0 µmol N L^{-1}, ~~average~~averaged 14.0±2.1 µmol N L^{-1}~~, and 0.42 – 0.84 µmol P L^{-1}, average 0.62±0.15 µmol P L^{-1}, respectively, ;Figure 3c).~~ in contrast, DIN concentrations at the same depth in other sites with deeper nutriclines ranged 6.5 to 12.1 µmol N L^{-1}, averaged 8.9±2.4 µmol N L^{-1} (Fig. 3c).

~~We also integrated~~The partitioned nutrient inventories (i.e., ~~NO_3^- and PO_4^{3-}~~ nutrient inventories ~~in both~~within the NDL and Ez) ~~at each station~~ also showed such a trend (Fig.~~ure~~ 4a & b~~):~~). The average Ez-inventory of DIN was 196±30 mmol N m^{-2} at stations with shallow nutriclines compared to 29±19 mmol N m^{-2} at other stations, and the average inventory of PO_4^{3-} (DIP) in the Ez at stations with shallow nutriclines was 13±1 mmol P m^{-2} compared to an average of 3±~~—~~2 mmol P m^{-2} at other stations. The pattern of nutrient inventories across stations possibly results from vertical water displacement induced by horizontal divergence at the mesoscale and/or basin scale (Du et al., 2021).

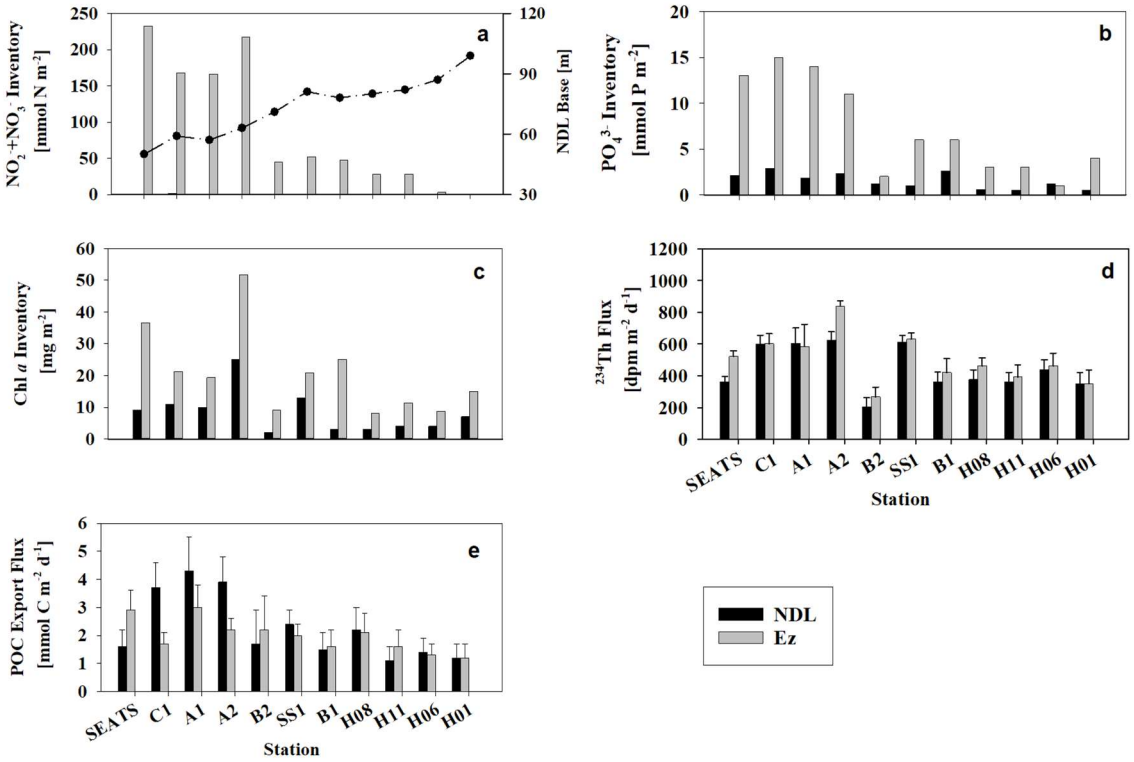

Figure 4: Integrated inventories of DIN (a) and DIP (b) in both the NDL (black) and Ez (grey). Also shown are the partitioned Chl *a* stocks (c), integrated partitioned ^{234}Th fluxes (d) and ^{234}Th-derived POC export fluxes (e). The high and low nutrient inventories correspond to shallow and deep nutriclines (a) (dotted line, NDL base), respectively.

Chl *a* concentrations at the 4 stations with shallower nutriclines were consistently enhanced in response to elevated nutrient levels resulting in shallower depths of subsurface Chl *a* maxima (SCM, Fig. 3d) relative to other stations (55-80 m vs 85-108 m). Chl *a* inventories at these stations with high nutrient inventories (23.6-52.2 mg m^{-2}, average 29.6±4.8 mg m^{-2}) were significantly higher ($p < 0.05$) than at others stations (8.0-22.8 mg m^{-2}, average 14.0±4.6 mg m^{-2}, Fig. 4c).

3.2 ^{234}Th and POC variability

Variations of total ^{234}Th and Chl *a* versus depth is shown in Fig. 5. The activities of total ^{234}Th ranged from 1.70±0.05 to 2.73±0.05 dpm L^{-1}, with an average of 2.30±0.31 dpm L^{-1}(n = 97, Fig. 5), and all stations displayed similar patterns. Generally, ^{234}Th was deficit relative to ^{238}U in the upper Ez, and was in equilibrium or excess at the base of and/or below Ez. The ^{234}Th deficit peaked within the NDL and largely diminished in the NRL, implying a large amount of particle removal occurred in the NDL but low export or high remineralization in NRL. The ^{234}Th activity minimum (1.70±0.17 dpm L^{-1}) appeared at a depth of 25 m at Station A1 (one of stations characterized by a shallow MLD and nutricline). ^{234}Th activity at the stations surrounding Station SS1 showed little spatial variability: the differences in ^{234}Th activity were less than 0.1 dpm L^{-1} at the same depth.

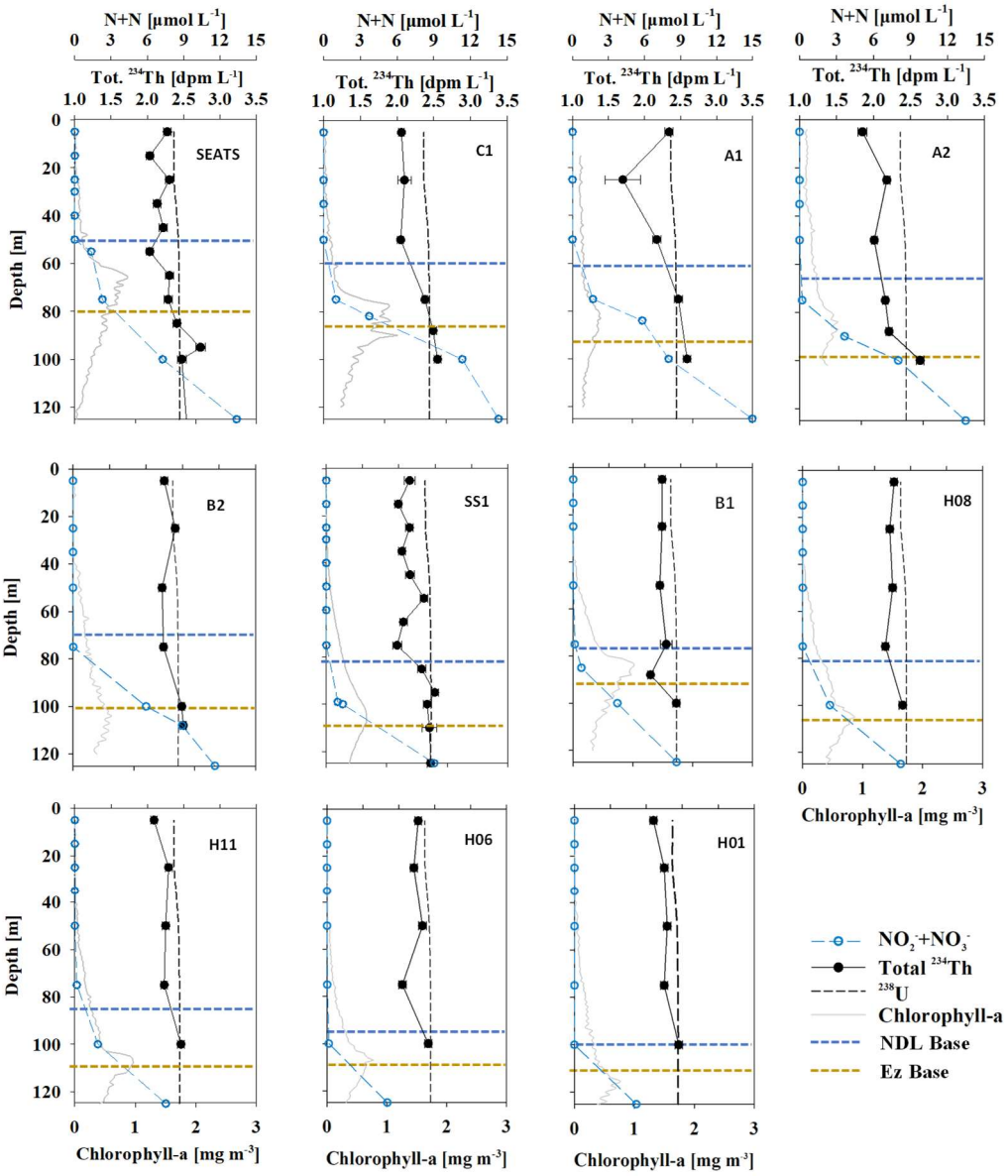

Figure 5: Depth profiles of DIN (blue open circle, μmol L^{-1}), total ^{234}Th activity (black dot, dpm L^{-1}), ^{238}U activity (black dash, dpm L^{-1}) and Chl *a* concentration (grey line, mg m^{-3}) in the South China Sea basin. The defined export horizons of the NDL base (blue dash) and Ez base (yellow dash) are also shown. The deficit of ^{234}Th relative to ^{238}U was the most pronounced in the province where DIN was too low to be detected.

Particulate ^{234}Th ranged from 0.13±0.01 dpm L^{-1} to 0.47±0.01 dpm L^{-1} (with an average of 0.25±0.11 dpm L^{-1}, n=83~~)~~~~(~~. Fig. 6). At most stations the profiles of particulate ^{234}Th shared similar depth patterns with Chl *a*, with the maximum values appearing in the subsurface water, while at stations H01 and H06, particulate ^{234}Th generally increased with depth in the upper

100 m, and showed little station to station variability. The maximum of particulate ^{234}Th appearing at both surface and subsurface at Station B2 suggested complicated biogeochemistry of ^{234}Th on particles.

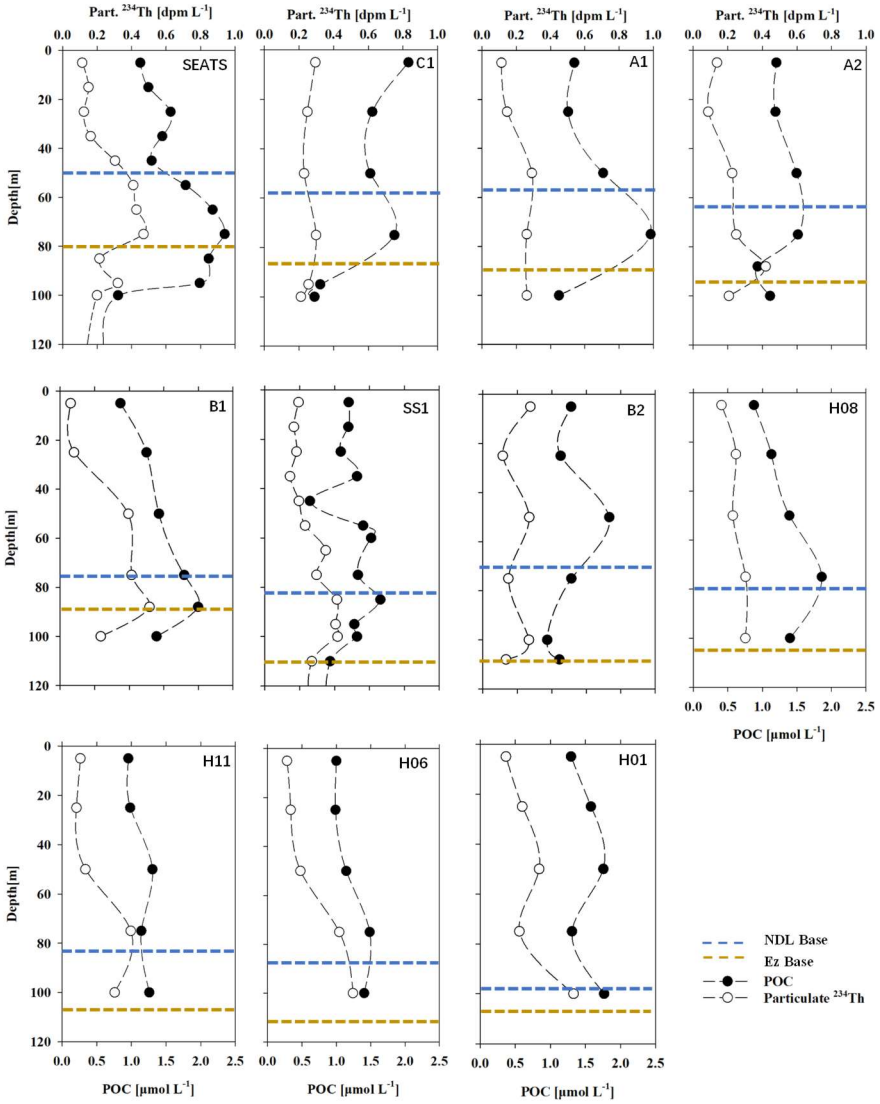

Figure 6: Profiles of POC (black dots, μmol L^{-1}) and particulate ^{234}Th activity (PTh, open circles, dpm L^{-1}) at all stations sampled in the South China Sea basin in June 2017. The bases of both the NDL (blue dashed line) and Ez (yellow dashed line) are also shown.

POC concentrations ranged from 0.83 μmol L^{-1} to 2.5 μmol L^{-1} (with an average of 1.2±0.44 μmol L^{-1}, n=83, Fig. 6). At most stations, the POC concentration was low (with an average of 1.1±0.2 μmol L^{-1}) in surface water and generally increased

with depth until reached its maximum at the SCM layer, and then decreased again with depth. However, at some stations (i.e., C1, B2), there were POC peaks appearing in both the surface water and the SCM layer.

3.3 ~~1D SS w~~Water column-integrated and sediment trap-derived ^{234}Th fluxes

Calculated ^{234}Th fluxes at different export horizons (i.e., NDL and Ez base) are shown in both Table 2 and Fig. 4d. ^{234}Th fluxes at the Ez base mostly ranged from 267±69 to 839±59 dpm m^{-2} d^{-1}. ^{234}Th fluxes at the NDL base ranged from 204±57 to 624±52 dpm m^{-2} d^{-1}, which accounts for 69-100% of ^{234}Th fluxes at the Ez base. We found that the ^{234}Th fluxes remained rather low, mostly <800 dpm m^{-2} d^{-1} during our study, which were close to the threshold for the validity of steady-state assumption as shown in many prior studies (e.g., Savoye et al., 2006; Resplandy et al., 2012). The sea surface Chl *a* also indicated that no bloom was observed during the survey in Jun. 2017 (Fig. S4), suggesting that the study area retained its biogeochemistry under the steady state condition.

^{234}Th fluxes at the Ez base ~~in this study~~ were within the ranges of ~~(~~62-1365 dpm m^{-2} d^{-1}, similar to those~~)~~ found in prior studies in the SCS basin (e.g., Cai et al., 2008; Cai et al., 2015; Zhou et al., 2013; Zhou et al., 2020a). Given that our high vertical resolution of sampling mode was only applied to stations SEATS and SS1, we estimated ^{234}Th fluxes at the Ez base by reducing the vertical resolution to a 25-m interval so as to be consistent with other stations, This exercise resulted in values of 490±60 and 655±71 dpm m^{-2} d^{-1} respectively for stations SEATS and SS1 compared to 522±43 and 631±48 dpm m^{-2} d^{-1} under the high-resolution sampling mode. The low-resolution sampling thus might induce an uncertainty of less than 6% for the ^{234}Th flux. However, high-resolution sampling is essential in order to examine the partitioning of carbon export in the upper water column, especially for the oligotrophic ocean characteristic of low export fluxes.

~~Although ^{234}Th fluxes at the base of the NDL have rarely been quantified, the particle-scavenging rate at any export horizon can be determined using ^{234}Th methodology (Buesseler et al., 2020b). ^{234}Th fluxes at the NDL base in the oligotrophic SCS (77-942, averaged 349±296 dpm m^{-2} d^{-1}) showed little difference from the integrated results of prior studies (Cai et al., 2015; Zhou et al., 2020a) due to the similarity of measured ^{234}Th activities in the NDL.~~ sBased on the high-resolution total ^{234}Th pattern at stations SEATS and SS1, we first determined ^{234}Th deficit in the NDL, showing substantial particle scavenging and POC export at the NDL base at both stations, and we subsequently found similar patterns at the rest of stations where estimated the partitioning in POC export fluxes.

Besides the ^{234}Th-^{238}U disequilibrium method, ~~S~~sediment trap-derived ^{234}Th fluxes at SEATS were 589±2 dpm m^{-2} d^{-1} at the NDL base (50 m), representing over 50% of the ^{234}Th flux, and 830±2 dpm m^{-2} d^{-1} near the Ez base (100 m). The trap-derived ^{234}Th fluxes were higher ~~than~~, but within 2-fold, ~~of~~ than the fluxes derived from bottle sampled ^{234}Th (362±34 dpm m^{-2} d^{-1} at 50 m and 471±46 dpm m^{-2} d^{-1} at 100 m) at both export horizons. Although ^{234}Th fluxes at the base of the NDL had rarely been quantified in prior studies, we estimated the particle-scavenging rate at the corresponding export horizon with the historical data of ^{234}Th. Our recalculation using these literature data showed that ^{234}Th fluxes at the NDL base averaged 349±296 dpm m^{-2} d^{-1} (n=36) with limited spatial and temporal variations in the oligotrophic SCS. This is also consistent with the fact that these prior measurements of ^{234}Th shared similarities in activities in the NDL (Cai et al., 2015; Zhou et al., 2020a).

Nevertheless, the partitioning in particle fluxes between NDL and Ez ~~particle fluxes~~, based on both techniques employed in this study, is similar, which further supports that our ^{234}Th-^{238}U disequilibrium-based fluxes are representative.

3.4 POC/^{234}Th ratios based on bottle filtration and sediment traps

Bottle-derived POC/^{234}Th profiles in the Ez are shown in Fig. 7. They ranged from 2.6 to 15.7 μmol dpm^{-1} (with an average of 5.6±3.3 μmol dpm^{-1}, N=83), peaked in the upper 25 m and generally decreased with depth at all stations. POC/^{234}Th differences between most stations gradually diminished with depth and converged near 4.2±1.6 μmol dpm^{-1} at the base of the Ez. The decreasing pattern of POC/^{234}Th was not observed at stations SEATS and H11 (as noted in Fig. 7a).

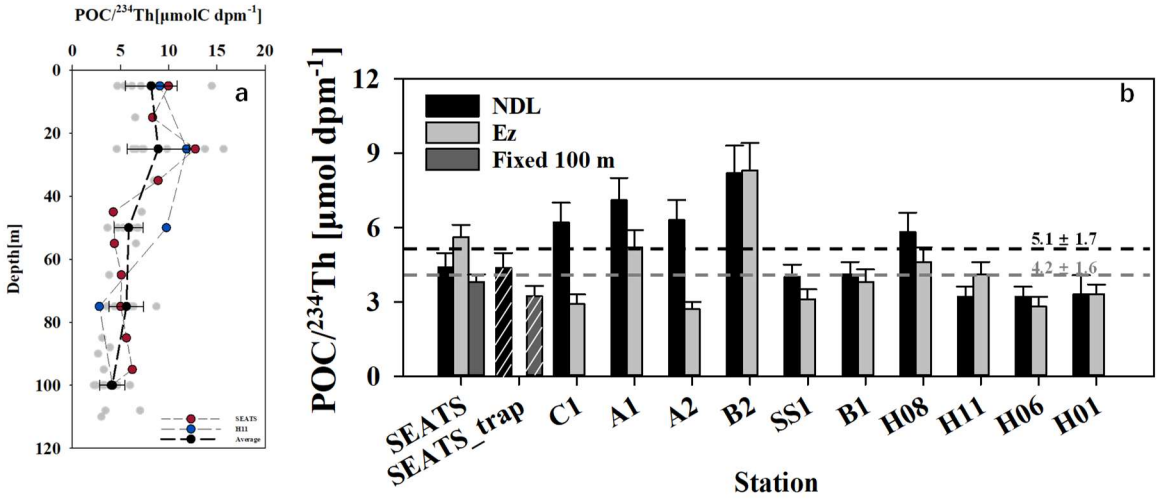

Figure 7: Water-column POC/ ^{234}Th ratios from bottle filtration, with the averages (black dots with dashed line) at each sampling depth plotted against depth (a). Also shown are the bottle- and trap-derived POC/ ^{234}Th ratios (bar with white stripes) at the bottom of the NDL (black), base of the euphotic zone (light grey), and fixed 100 m depth (dark grey) (b). Generally, the variability of POC/^{234}Th decreased as depth increased and converged around 4.2±1.6μmol dpm^{-1} at the Ez base. No significant variability (within 2-fold) was found between POC/ ^{234}Th ratios derived from bottle and trap samples accessed at the same sampling depths at station SEATS.

POC/^{234}Th ratios from sediment traps were only measured at Station SEATS, and were 4.7 and 3.2 μmol dpm^{-1} at 50 and 100 m, respectively (Fig. 7b). These values are comparable with the bottle-derived POC/^{234}Th ratios from the same site during the cruise.

3.5 $\delta^{15}N_{PN}$ from sediment traps

The $\delta^{15}N_{PN}$ values for the trap samples varied between 2.6‰ to 6.7‰ in the upper 200 m at stations SEATS and SS1, showing an increasing trend with depth. Specifically, the ~~lightest~~ lowest $\delta^{15}N_{PN}$ of 2.6 ‰ was observed at 50 m within the NDL, and the $\delta^{15}N_{PN}$ increased to 4.7‰ at the Ez base (about 100 m). Below the Ez, the $\delta^{15}N_{PN}$ value increased to 6.7‰ at 200 m at Station SEATS. A similar pattern of $\delta^{15}N_{PN}$ was also found at Station SS1, with the lowest~~lightest~~ $\delta^{15}N_{PN}$ of 4.1 ‰ at 50 m, an intermediate value of 5.8~~0~~ ‰ at 100 m and the ~~heaviest~~ highest value of 6.0~~0~~ ‰ at 200 m. The observed $\delta^{15}N_{PN}$ values at both stations were comparable to previous results (3.3-7.3 ‰) from sinking particles collected by sediment traps in the upper 500 m around Station SEATS (Kao et al., 2012; Yang et al., 2017). Yang et al. (2017) found a $\delta^{15}N_{PN}$ value of 4.9‰ at 100 m at station SEATS, which was very consistent with our observation at the same depth of Station SEATS. These results suggest that inter-annual variations in $\delta^{15}N_{PN}$ from the upper ocean in the SCS may be limited, and the $\delta^{15}N_{PN}$ value at Station SS1 from the cruise in 2019 could be comparable to that in this campaign. We thus diagnose the nutrient sources of sinking particles at stations with different environmental settings without focusing on temporal variability.

4 Discussion

4.1 ^{234}Th fluxes at the NDL and Ez bases

~~Assuming a 1D-SS model is valid in the case of low particle fluxes (^{234}Th flux < 800 dpm m^{-2} d^{-1}, Savoye et al., 2006), t~~The ~~partitioned~~ particle flux at the NDL base was comparable (88±11%) to that at the Ez base. This vertical structure indicates that the NDL base should be a hotspot for particle scavenging. The trap-derived ^{234}Th fluxes (589±2 dpm m^{-2} d^{-1} at 50 m and 830±2 dpm m^{-2} d^{-1} at 100 m) were slightly higher compared to bottle-derived ^{234}Th fluxes (362±34 dpm m^{-2} d^{-1} at 50 m and 471±46 dpm m^{-2} d^{-1} at 100 m). The higher trap-derived ^{234}Th fluxes might possibly be related to incomplete removal of zooplankton (Buesseler et al., 2020b). In addition, the ~~inconsistency~~ discrepancy ~~between~~ in ~~the two methods~~between could be due to the difference in their~~t~~ time scales (Umhau et al., 2019). Regardless of the differences in ^{234}Th flux estimations from the separate methods, the similar vertical partitioning from ~~the~~ both bottle- and trap-derived ^{234}Th fluxes indicated substantial particle scavenging at the bases of both the NDL and Ez in the oligotrophic SCS.

It is also interesting to note that at stations with higher nutrient inventories, ^{234}Th fluxes (362±34-624±52 dpm m^{-2} d^{-1}, average 547±107 dpm m^{-2} d^{-1} at the NDL base and 522±45-839±59 dpm m^{-2} d^{-1}, average 637±120 dpm m^{-2} d^{-1} at the Ez base) are significantly higher (by approximately 100-200 dpm m^{-2} d^{-1}) than those at other stations (210±38-520±31 dpm m^{-2} d^{-1}, average 359±90 dpm m^{-2} d^{-1} at the NDL base, and 204±57-613±42 dpm m^{-2} d^{-1}, average 427±105 dpm m^{-2} d^{-1} at the Ez base, Fig. ~~5~~4~~e~~d). This regional pattern of ^{234}Th fluxes might result from differences in nutrient distributions, as ^{234}Th has thus far been an indispensable tool to trace biogenic particle scavenging (Ceballos-Romero et al., 2022 and references therein). Whether

these high and low ^{234}Th fluxes would respectively drive similar POC export fluxes at stations with high and low nutrient inventories remains to be determined.

4.2 POC/^{234}Th ratio and ^{234}Th-derived POC fluxes in the SCS basin

4.2.1 Variability in bottle- and trap-derived POC/^{234}Th ratios

Determining POC/^{234}Th ratios on particles at the export horizons is essential for converting ^{234}Th fluxes to POC export fluxes. POC/^{234}Th ratios can, however, vary three orders of magnitude between different regions, depths, seasons and even particle sizes (Buesseler et al., 2006; Puigcorbé et al., 2020). The variability in POC/^{234}Th is possibly due to the combined effect of particle generation, aggregation, remineralization, and particulate ^{234}Th decay (Cai et al., 2006). As shown in Fig. 7a, water-column POC/^{234}Th ratios decreased gradually with depth and varied within 5 μmol dpm^{-1} below the 50 m. This decreasing tendency of POC/^{234}Th ratios was highly consistent with results from prior studies conducted in tropical-subtropical oligotrophic ecosystems despite differing sampling devices (Puigcorbé et al., 2020). The maximum ratio with the highest variability was observed in the upper 25 m, at a depth where primary production usually peaks in oligotrophic ecosystems (Xie et al., 2018; Buesseler et al., 2020b). Even though POC/^{234}Th ratios determined from bottle filtration were variable in prior studies, they are strongly coupled to ratios from sediment traps (Gustafsson et al., 2013), which are considered to represent the ratio on sinking particles. POC/^{234}Th ratios based on bottle filtration and sediment traps in this study were also compared to each other at the same depth at Station SEATS: The POC/^{234}Th ratios were 4.2 and 3.2 μmol dpm^{-1} on trap samples at 50 and 100 m, similar to bottle-filtration derived POC/^{234}Th ratios (4.4±0.6 and 3.8±0.6 μmol dpm^{-1} at 55 and 100 m, respectively). Besides bottle- and trap-derived POC/^{234}Th ratios, the POC/^{234}Th ratio on large-size particles (> 53 μm and assumed to be sinking particles, Buesseler et al., 2006) retrieved from *in situ* pumping also decreased with depth at Station SEATS (Cai et al., 2006) and converged to a narrow range from 1.8 to 4.1 μmol dpm^{-1} at 100 m in the SCS basin (Chen, 2008). We thus confirmed that bottle-derived POC/^{234}Th was comparable with those derived from sinking particles accessed from traps or *in situ* pumps. This is consistent with prior studies showing that POC export fluxes based on bottle POC/^{234}Th were comparable with trap POC fluxes (e.g., Zhou et al., 2020a). Due to a lack of trap or pump deployment at all sites, and considering the similarity of POC/^{234}Th ratios using different methodologies, POC/^{234}Th ratios based on bottle filtration were used for POC flux estimation.

POC/^{234}Th ratios at the Ez base varied from 2.8±0.4 to 8.3±0.7 μmol dpm^{-1} (averaged 4.2±1.6 μmol dpm^{-1}, Fig. 7b), which is comparable with previously published results (e.g., 1.6 to 5.3 μmol dpm^{-1}, averaged 4.2±1.6 μmol dpm^{-1}) from the SCS basin (Cai et al., 2015; Zhou et al., 2013; Zhou et al., 2020a). POC/^{234}Th ratios at the NDL base were generally higher than those at Ez base, ranging from 3.2±0.4 to 8.2±1.1 μmol dpm^{-1} (averaged 5.1±1.7 μmol dpm^{-1}).

We found that variability in POC/^{234}Th ratios was insignificant between stations with shallow and deep nutriclines: The POC/^{234}Th ratio at the NDL base ranged from 4.4±0.6 to 7.1±0.9, averaged 6.0±1.0, μmol dpm^{-1} at stations with shallow nutriclines (i.e., Sta. SEATS, C1, A1 and A2), which was slightly higher than the values at other sites (ranged from 3.2±0.4 to

8.2±1.1, averaged 4.5±1.7 μmol dpm^{-1}). On the other hand, the POC/^{234}Th ratios at the Ez base ranged from 2.9±0.4 to 5.5±0.7, averaged 4.0±1.3 μmol dpm^{-1} at stations with shallow nutriclines, which was like the POC/^{234}Th ratios at other sites (ranged from 2.8±0.4 to 8.3±1.1, averaged 4.3±1.7 μmol dpm^{-1}). The relatively low POC/^{234}Th at the NDL base at stations with deep nutriclines may be explained by higher particle remineralization rates with increasing depth. Based on similar ranges of ^{234}Th fluxes and POC/^{234}Th ratios, the estimated POC export fluxes in this study were consistent with prior studies in the SCS basin (Cai et al., 2015; Zhou et al., 2020a).

4.2.2 POC export fluxes at different export horizons

POC export fluxes were estimated after combining the partitioned ^{234}Th fluxes and POC/^{234}Th ratios. ^{234}Th-derived POC export fluxes ranged from 1.2±0.5 to 3.0±0.8 mmol C m^{-2} d^{-1} at the base of the Ez, and from 1.2±0.6 to 4.3±1.2 mmol C m^{-2} d^{-1} at the base of the NDL (Fig. 4e and Table 2). POC export fluxes estimated in this study are of the same order of magnitude as previous estimates in the SCS basin (Zhou et al., 2013; 2020a; Cai et a., 2015).

To assess the POC export flux using different methods, we compared ^{234}Th- and trap-derived POC export fluxes at station SEATS. POC export fluxes were comparable near the Ez base (2.9±0.9 and 2.7±0.3 mmol C m^{-2} d^{-1} for ^{234}Th- and trap-derived, respectively). However, the ^{234}Th-derived POC export flux of 1.6±0.6 mmol C m^{-2} d^{-1} was slightly lower than the trap-derived POC export flux (2.8±0.3 mmol C m^{-2} d^{-1}) at 50 m at Station SEATS. The lower ^{234}Th-derived POC export flux at 50 m may indicate potential contamination by organics in the traps (e.g., swimmers) that would result in higher measured POC fluxes in the oligotrophic SCS basin. A recent study of the EXPORTS program found that swimmers could increase the measured POC export flux by 2-fold in the traps (Estapa et al., 2021). Although slight disagreement between different methods was often noted and difficult to assign causes (Hung and Gong, 2007; Stewart et al., 2007; Lampitt et al., 2008; Haskell II et al., 2013; Buesseler et al., 2020b), we clearly found substantial POC export fluxes at the NDL base that were comparable to those at the Ez base in the SCS. A recent study based on ^{234}Th and sediment traps in the oligotrophic Gulf of Mexico also found particle production dominates in the upper Ez (0-60 m) where nutrients are depleted (Stukel et al., 2021). The results above conflict with previous knowledge suggesting that POC export flux from the nutrient-depleted mixed layer is extremely low (Coale and Bruland, 1987). The substantial POC export flux at the NDL base was highly correlated to the Chl *a* inventory, an index of biomass in the corresponding layer (Fig. 8a). In this regard, the sources of new nutrients that support the relatively high biomass in the NDL and drive the POC export fluxes at the NDL base in the SCS basin need to be constrained.

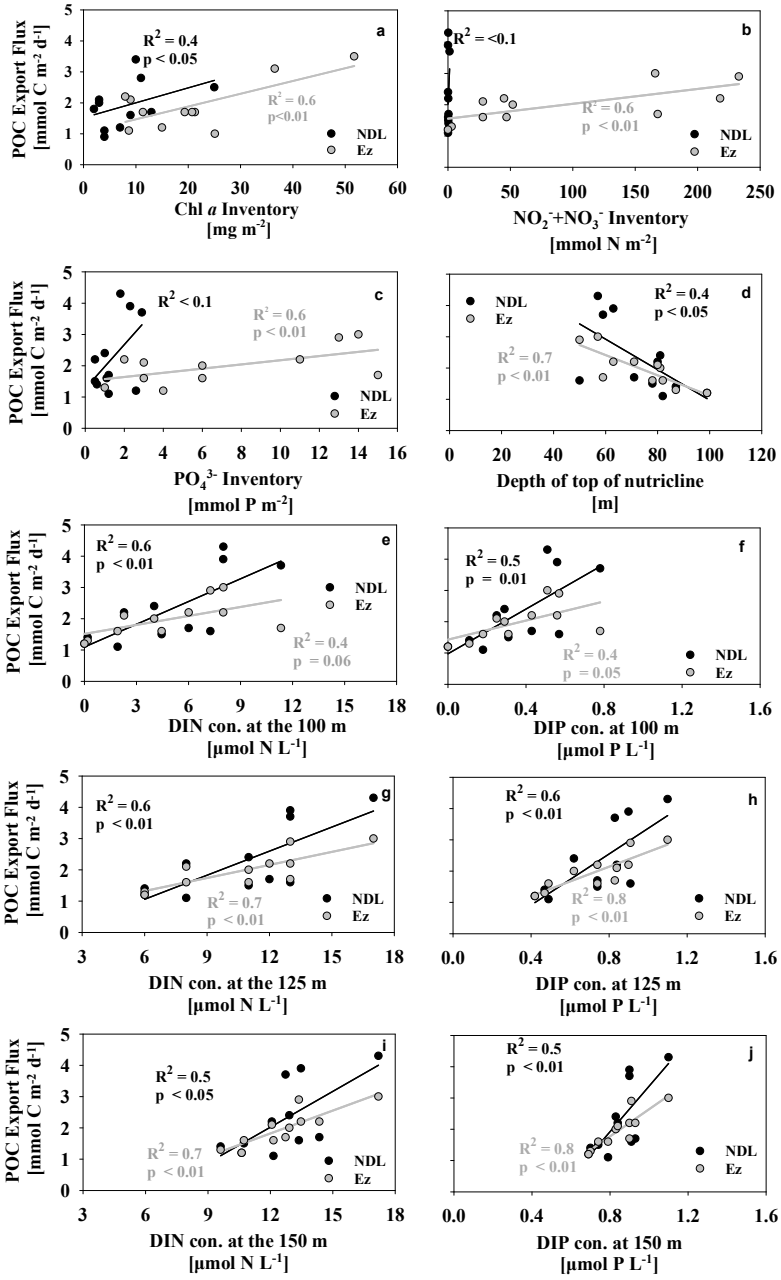

460

Figure 8: Relationship between POC export flux at the NDL base (black dots) and Ez base (grey dots) vs. Chl *a* (a), DIN (b) and DIP inventories (c) in the corresponding layers. Also plotted are the relationships between the depth of the top of the nutricline (d), and DIN and DIP concentrations in subsurface water at 100, 125 and 150 m versus partitioning POC export fluxes (e-j).

4.3 Diagnosis of nutrient sources supporting particle export in the oligotrophic SCS

4.3.1 Correlation between POC export flux and subsurface nutrient concentrations

To diagnose the nutrient sources that support ~~substantial~~ POC export fluxes at different export horizons, we examined the relationship between partitioned POC export fluxes and nutrient inventories in corresponding layers. Nutrient stocks might regulate POC export fluxes at the Ez base based on their positive correlation (Fig. 8b & c). However, a ~~relatively~~ poor relationship between POC export fluxes at the NDL base and nutrient inventories in the NDL was found, which suggests that the *in situ* nutrients in the NDL interior are insufficient to support the POC export from this horizon.

~~Since *in situ* nutrients in the NDL were insufficient to support POC export flux at the NDL, o~~Other external nutrient sources ~~likely~~ must thus influence~~d~~ POC export flux in the nutrient-deleted ecosystems. Episodic events (e.g., eddies and typhoons) that can transport subsurface nutrients into nutrient-deficient regimes have been confirmed in other oligotrophic ocean regions (Johnson et al., 2010; Zhou et al., 2020b). Mesoscale eddies can pump subsurface nutrient-rich waters into the upper Ez and enhance surface Chl *a* based on a long-term dataset of the Chl *a* anomaly corresponding to eddy properties (e.g., SLA, amplitude and eddy rotation speed) in the oligotrophic SCS (He et al., 2016). Besides Chl *a*, POC concentrations and ^{234}Th deficits relative to ^{238}U were also significantly enhanced in the upper 25 m by impacts from cyclonic eddies in the oligotrophic SCS where the nutrient concentrations were observed to be quite low (Zhou et al., 2020b). This enhancement of biomass would be amplified by the interplay of typhoons and cyclonic eddies (Liu et al., 2019). ^{15}N-isotopic results also indicate that subsurface nitrate is an important external nutrient impacting export production (Yang et al., 2017). The nutrients from underlying waters may thus play an important role in supporting POC export from the NDL.

As the potential availability of subsurface nutrients was determined by the depth of the nutricline and the nutrient concentration in subsurface waters (Moutin and Raimbault, 2002; Mouriño-Carballido et al., 2021), we ~~subsequently~~ examined relationships between partitioned POC export fluxes and the depth of the top of the nutricline, and subsurface DIN and DIP concentrations below the Ez at 100, 125 and 150 m where biological uptake might be negligible (Fig. 8d-j). The moderately positive correlation ($R^2 = 0.4$, $p < 0.05$) between the depth of the top of the nutricline and POC export fluxes at the NDL base (Fig. 8d) suggests that shallower nutriclines could indeed ~~might~~ facilitate subsurface nutrient intrusion into the upper Ez, and subsequently stimulate higher POC export fluxes in the upper nutrient-depleted ecosystems. Besides the nutricline, POC export fluxes at the NDL base were also correlated ($R^2 \geq 0.4$) with DIN and DIP concentrations in the subsurface water near or below the Ez base (Fig. 8e-j). The positive relationship thus suggests that POC export fluxes in the upper nutrient-depleted Ez are also highly associated with subsurface nutrient levels.

It is also noteworthy that the timescale of ship-based nutrients data is instantaneous, which may differ from the timescale of ^{234}Th method of weeks to months. Consequently, the correlations between *in situ* nutrients and ^{234}Th-derived POC fluxes may be misinterpreted by the difference in timescales. To further investigate the correlations between nutrients and ^{234}Th-derived POC fluxes, ^{234}Th-derived POC fluxes were also related to the model-derived monthly average of nutrients (i.e., DIN concentration and the depth of nutricline, Du et al., 2021) during summer (Fig. S5). The correlations between the two

parameters showed to be statistically significant (P<0.05), again implying the importance of nutrient modulation on export fluxes. Taken together, we confirm that subsurface nutrients significantly influence the POC export flux at the NDL base.

4.3.2 Nutrient sources diagnosed via ^{15}N-isotopic mass balance

As the timescale of ^{234}Th-^{238}U disequilibrium was not instantaneous, any episodic intrusion events before sampling (~ 20 days) could be recorded. Due to the limited Kuroshio intrusion into the SCS basin during the summer and extremely low levels of nutrients in the surface Kuroshio current (Du et al., 2013), the minor lateral transport of nutrients by Kuroshio waters could not supplybe neglected new N over the study area (Du et al., 2013). Thus, we assume that air-derived nitrogen (i.e., NF nitrogen fixation and atmospheric nitrogen deposition [AND]) and upwelled nitrate are the major sources of new N supporting PN corresponding POC export out of the NDL and at the Ez base. Using a two-endmember mixing model based on the ^{15}N-isotopic balance (Kao et al., 2012; Böttjer et al., 2017), we can evaluate the relative contribution of these two plausible sources of new N to support the particle export at sites SEATS and SS1 using the following equations:

$$1= f_{NO_3^-} + f_{Air} \quad (10)$$

$$\delta^{15}N_{PN} = \delta^{15}N_{NO_3^-} \times f_{NO_3^-} + \delta^{15}N_{air} \times f_{air} \quad (11)$$

where, $f_{NO_3^-}$ and f_{Air} represent the fraction of PN export contributed by upwelled DIN from the subsurface and by air-derived nitrogen from nitrogen fixation and atmospheric nitrogen deposition, respectively. $\delta^{15}N_{NO_3^-}$ and $\delta^{15}N_{air}$ denote the endmembers of $\delta^{15}N$ for subsurface DIN and air-derived N, respectively. $\delta^{15}N_{Air}$ is chosen as -1.1‰ by considering the influences of both nitrogen fixation and atmospheric nitrogen deposition following Yang et al. (2022). The $\delta^{15}N_{NO_3^-}$ values of subsurface DIN in the SCS basin are found to be unchanged spatially and temporally, with an average of 4.7±0.4‰ at 100 m (Yang et al., 2017; Yang et al., 2022).

~~where F_{PN}, $F_{NO_3^-}$ and F_{Air} represent, the fluxes of total PN, PN contributed by upwelled DIN from the subsurface and nitrogen from the atmosphere (i.e., N_2 fixation and AND), respectively, and $\delta^{15}NO_3^-$ and $\delta^{15}N_{Air}$ denote the endmembers of $\delta^{15}N$ for DIN in subsurface waters and air-derived N, respectively.~~

$f_{NO_3^-}$ was estimated to be about 59-67% at the NDL base, and 86-98% at the Ez base at Station SEATS. The proportion was higher (84-96%) at 50 m within the NDL and nearly 100% at 100 m close to the Ez base at Station SS1. The differences in isotopic compositions of $\delta^{15}N_{PN}$ in the NDL are likely related toshould be a function of the relative contributions of nutrient sources. Little variability in the regional NF nitrogen fixation rate suggests that differences in nitrogen fixationNF would not

lead to such a discrete pattern of $\delta^{15}N_{PN}$ ~~compositions~~ near the NDL base between sites, except when influenced by Kuroshio waters (Lu et al., 2018). However, Gao et al. (2020) clarified the spatial ~~variability~~ variation ~~in~~of atmospheric nitrogen deposition ~~AND~~ in the SCS basin showing the aerosol NO_3^- concentration at Station SEATS ~~is~~ was nearly twice that at Station SS1 which ~~lies~~ is relatively far away from the continent. In addition, three anti-cyclonic eddies (Fig. ~~S4~~S6) influenced the water surrounding Station SS1 before our visit in this region. In this regard, the relatively elevated contribution of subsurface DIN at Station SS1 might be attributed to the decrease in atmospheric nitrogen deposition~~AND~~ and event-driven subsurface DIN intrusion. Despite the variability of $\delta^{15}N_{PN}$ between stations, our results suggested a major contribution of subsurface DIN in the SCS basin based on the isotopic balance. These estimates indicate that POC export fluxes supported by subsurface DIN are ~~comparable~~ sufficient, and even more important than those supported by nitrogen fixation and atmospheric nitrogen deposition ~~NF and AND~~ at the base of NDL where the DIN concentration is usually below detection. To validate our ^{15}N-~~estimates~~ based estimates~~on the ^{15}N-isotopic balance~~, we ~~also~~ compared the reported fluxes of nitrogen fixation and atmospheric nitrogen deposition ~~NF and AND~~ in the SCS basin to the measured PN fluxes from the sediment trap at 50 m (about 2.8 mmol C m^{-2} d^{-1} and 0.42 mmol N m^{-2} d^{-1}, assuming a C/N ratio of 6.6 in sinking particles) at Station SEATS in this study. The average nitrogen fixation~~NF~~ rate was 0.06 mmol N m^{-2} d^{-1} (Kao et al., 2012; Chen et al., 2014) and the atmospheric nitrogen deposition flux ~~AND~~ was 0.14 mmol N m^{-2} d^{-1} (Yang et al., 2014; Kim et al., 2014). The contribution of nitrogen fixation and atmospheric nitrogen deposition~~NF and AND~~ to the measured PN flux at 50 m is estimated to be 48%. This mass-based estimate is consistent with the results derived from the isotopic balance, suggesting a major role of subsurface nutrients in supporting POC export from the NDL base. ~~,~~ Furthermore,

~~T~~the differences in $\delta^{15}N_{PN}$ at both stations SEATS and SS1 gradually disappeared with increasing depth because the new nutrients were predominantly sourced from the nutrient-rich subsurface waters near the base of the Ez. This enhanced contribution of subsurface ~~nutriens~~ nutrients is consistent with results from prior studies (Kao et al., 2012; Yang et al., 2017) that ~~indicate~~ subsurface nutrients contribute to more than 90% of the export production at the Ez base in the SCS basin.

Taken together, ~~To validate our estimates based on the ^{15}N-isotopic balance, we also compared the reported fluxes of NF and AND in the SCS basin to the measured PN fluxes from the sediment trap at 50 m (about 2.8 mmol C m^{-2} d^{-1} and 0.42 mmol N m^{-2} d^{-1}, assuming a C/N ratio of 6.6 in sinking particles) at station SEATS in this study. The average NF rate was 0.06 mmol N m^{-2} d^{-1} (Kao et al., 2012; Chen et al., 2014) and the AND was 0.14 mmol N m^{-2} d^{-1} (Yang et al., 2014; Kim et al., 2014). The contribution of NF and AND to the measured PN flux at 50 m is estimated to be 48%. This mass-based estimate is consistent with the results derived from the isotopic balance.~~

~~In summary, we conclude that, compared to external N inputs from the atmosphere, nutrient intrusion from the subsurface is one of the major contributors supporting POC export fluxes at the NDL base in the oligotrophic SCS basin, and NF and AND may also contribute substantially to POC export flux at the NDL base.~~

~~W~~we thus ~~speculate~~ hypothesize that the episodic event-driven nutrient upwelling from the subsurface to the surface nutrient-depleted ecosystem stimulates the growth of planktonic organisms and elevates the particle scavenging rate in the oligotrophic SCS, which could be reflected in the ^{234}Th whose activities integrate the impacts of processes occurring over

several months. It is also worthwhile considering the influences from mesoscale and sub-mesoscale processes in the SCS basin. Prior studies showed the concurrence of the vertical transport of particles supported by locally uplifted nutrients and the horizontal transport of particles supported by the nutrients trapped in eddies (Wang et al., 2018, Ma et al., 2021). In this study, we found enhanced POC export fluxes at stations with high nutrient inventories and inferred that the POC export fluxes might also be supported by nutrients from the subsurface waters based on the signal of $\delta^{15}N_{PN}$. However, our current study was unable to diagnose the pathways of nutrients fuelling the primary and export production, which needs further studies.

5 Conclusions

With the aid of high depth resolution ^{234}Th sampling, ^{234}Th and POC fluxes at both the NDL and Ez bases were estimated in the oligotrophic SCS basin during the summer of 2017. Although DIN was exhausted in the NDL, ^{234}Th-based POC export fluxes at the NDL base were estimated to be 1.1±0.5- to 4.3±1.2 mmol C m^{-2} d^{-1}, which is comparable to those at the Ez base (1.2±0.5- to 3.0±0.8 mmol C m^{-2} d^{-1}). The relationship between POC export flux and nutrients was diagnosed: spatially, the POC export flux at the Ez base was elevated at stations with shallow nutriclines, corresponding to high nutrient inventories (1.7±0.4- to 3.0±0.8 mmol C m^{-2} d^{-1}) relative to stations with low nutrient inventories (1.2±0.5- to 2.2±1.2 mmol C m^{-2} d^{-1}). More than 50% of the relatively high particle export occurring at the NDL base was verified by N-isotopes to be supported by DIN from the subsurface. It thus indicated that other pathways (e.g., episodic events) might be important for nutrient intrusion into the Ez. The higher POC export flux resulted from shallow-nutricline derived higher nutrient stocks and biomass in the Ez. We thus hypothesize that subsurface nutrients might act as the primary regulator of POC export fluxes at both the Ez and NDL bases on a seasonal timescale. The reduced export flux under the background of higher surface temperature and stronger stratification further implies that sea surface warming might lower the efficiency of ~~the biological pump~~BCP.

Data Availability.

All data accessed from *in situ* observations (i.e., temperature, salinity, fluorescence-based Chl *a*, ^{234}Th, POC and nutrients) are currently for review and will be available at National Science Data Bank (https://www.scidb.cn/en) with DOI. DOI number will be provided before the acceptance of this manuscript. The speeds of horizontal water current from May to August, 2017 and 2019 were obtained from the Copernicus Marine Environment Monitoring Service (CMEMS, https://marine.copernicus.eu/). The vertical speeds of water current and diffusive (*Kz*) was derived from China Sea Muti-Scale Ocean Modeling System (CMOMS, https://odmp.ust.hk/cmoms/).

Supplement.

Additional figures referenced in text: **Figure S1**. Relationship between bottle-derived Chl a (Y-axis) and CTD fluorescence-based Chl a (X-axis). **Figure S2**. Surface distribution of monthly sea level anomalies (SLA, a) and eddy kinetic energy (EKE, b) with water currents during the cruise determined from modeling work. The SLA and EKE indicated stations SEATS, A1 and C1 experienced impacts of the mesoscale eddies. **Figure S3**. Climatological sea surface temperature anomalies in the SCS during June from the China Sea Multi-scale Ocean Modeling System (CMOMS). Stations C1 and A2, impacted by cold water sourced from the southwest SCS basin during the survey, are shown. ~~**Figure S4**. Surface distributions of monthly sea level anomalies (SLA) during the summer of 2019 with water currents from modeling work. The SLA show that station SS1 was impacted by mesoscale processes for at least one week before our visit (July 13th, 2019).~~**Figure S4**. Satellite-derived the 8-day averaged surface Chl *a* in the SCS basin during June 2017, showing that sea surface Chl *a* concentration was little enhanced during our ship-based sampling period. Note that Station A1 was visited after typhoon Merbok, which was generated on June 9, 2017 at 13.1°N, 119.8°E in the southern China Sea. Merbok landed on June 12 at 27.5°N, 117.3°E. **Figure S5**. Relationship between POC export fluxes at the NDL base (black dots) and Ez base (grey dots) vs. the model-derived depth of the top of the nutricline (top) and DIN concentration in the subsurface water at 100 m (bottom). **Figure S46**. Surface distributions of monthly sea level anomalies (SLA) during the summer of 2019 with water currents from modeling work. The SLA show that station SS1 was impacted by mesoscale processes for at least one week before our visit (July 13th, 2019). **Table S1**. The list of total and particulate ^{234}Th activity and POC concentration at sampling depth at stations.

Competing interests.

The authors declare that they have no conflict of interest.

Author contribution.

All authors have been involved in the writing of the paper and have approved the final submitted manuscript. Yifan Ma and Minhan Dai are major contributors to the study's conception, data analysis and drafting the paper. Kuanbo Zhou, Weifang Chen and Junhui Chen contributed significantly to cruise design, sample collections and/or data acquisition. Jin-Yu Terence Yang contributed substantially to isotopic data acquisition and analysis.

Acknowledgements.

This study was funded by the National Natural Science Foundation of China through grants No. 41890800 and 42188102, and by the National Basic Research Program of China (973 Program) through grant No.2015CB954000. Yifan Ma was supported

by a PhD Fellowship from the State Key Laboratory of Marine Environmental Science, Xiamen University. We thank Drs. Xianghui Guo, Peng Cheng and Yuyuan Xie who led the cruise as chief scientists, and Bangqing Huang with his group assisted Chloropyll-a data analysis. Zhongwei Yuan, Lifang Wang and Tao Huang are thanked for nutrient sampling and analysis. Silin Ni and Liguo Guo are thanked for helping with the collection of particulate samples. Qing Li and Li Tian are also thanked for beta and POC/PN analyses, respectively. Yangyang Zhao, Zhongwei Yuan and Chuanjun Du are thanked for their valuable comments. We are grateful to the crew of the R/V Tan Kah Kee along with its staff for their help during the cruise.

References

Barone, B., Church, M. J., Dugenne, M., Hawco, N. J., Jahn, O., White, A. E., John, S. G., Follows, M. J., DeLong, E. F., Karl, D. M.: Biogeochemical dynamics in adjacent mesoscale eddies of opposite polarity. Global Biogeochem Cycles, 36: e2021GB007115, https://doi.org/10.1029/2021GB007115, 2022.

Benitez-Nelson, C. R., Buesseler, K. O., Crossin, G.: Upper ocean carbon export, horizontal transport, and vertical eddy diffusivity in the southwestern Gulf of Maine. Cont Shelf Res, 20: 707-736, https://doi.org/10.1016/S0278-4343(99)00093-X, 2000.

Benitez-Nelson, C. R., Buesseler, K. O., Van Der Loeff, M., Andrews, J., Ball, L., Crossin, G., Charette, M.: Testing a new small-volume technique for determining ^{234}Th in seawater. Journal of Radioanalytical Nuclear Chemistry, 248: 795-799, https://doi.org/10.1023/a:1010621618652, 2001.

Böttjer, D., Dore, J. E., Karl, D. M., Letelier, R. M., Mahaffey, C., Wilson, S. T., Zehr, J., Church, M. J.: Temporal variability of nitrogen fixation and particulate nitrogen export at Station ALOHA. Limnol Oceanogr, 62: 200-216, https://doi.org/10.1002/lno.10386, 2017.

Buesseler, K. O., Bacon, M. P., Cochran, J. K., Livingston, H. D.: Carbon and nitrogen export during the JGOFS North Atlantic Bloom experiment estimated from ^{234}Th: ^{238}U disequilibria. Deep-Sea Res Part I, 39: 1115-1137, https://doi.org/10.1016/0198-0149(92)90060-7, 1992.

Buesseler, K. O., Benitez-Nelson, C. R., Moran, S., Burd, A., Charette, M., Cochran, J. K., Coppola, L., Fisher, N., Fowler, S., Gardner, W.: An assessment of particulate organic carbon to thorium-234 ratios in the ocean and their impact on the application of ^{234}Th as a POC flux proxy. Mar Chem, 100: 213-233, https://doi.org/10.1016/j.marchem.2005.10.013, 2006.

Buesseler, K. O., Boyd, P. W., Black, E. E., Siegel, D. A.: Metrics that matter for assessing the ocean biological carbon pump. Proc Natl Acad Sci U S A, 117: 201918114, https://doi.org/10.1073/pnas.191811411, 2020a.

Buesseler, K. O., Benitez-Nelson, C. R., Roca-Martí, M., Wyatt, A. M., Resplandy, L., Clevenger, S. J., Drysdale, J. A., Estapa, M. L., Pike, S., Umhau, B. P.: High-resolution spatial and temporal measurements of particulate organic carbon flux using thorium-234 in the northeast Pacific Ocean during the EXport Processes in the Ocean from RemoTe Sensing field campaign. Elementa: Science of the Anthropocene, 8, https://doi.org/10.1525/elementa.2020.030, 2020b.

Cai, P., Chen, W., Dai, M., Wan, Z., Wang, D., Li, Q., Tang, T., Lv, D.: A high-resolution study of particle export in the southern South China Sea based on ^{234}Th: ^{238}U disequilibrium. J Geophys Res-Oceans, 113: C04019 https://doi.org/10.1029/2007JC004268, 2008.

Cai, P., Dai, M., Chen, W., Tang, T., Zhou, K.: On the importance of the decay of ^{234}Th in determining size-fractionated C/^{234}Th ratio on marine particles. Geophys Res Lett, 33: L23602 https://doi.org/10.1029/2006GL027792, 2006.

Cai, P., Zhao, D., Wang, L., Huang, B., Dai, M.: Role of particle stock and phytoplankton community structure in regulating particulate organic carbon export in a large marginal sea. J Geophys Res-Oceans, 120: 2063-2095, https://doi.org/10.1002/2014JC010432, 2015.

Ceballos-Romero, E., Buesseler, K. O., Villa-Alfageme, M.: Revisiting five decades of 234 Th data: a comprehensive global oceanic compilation. Earth Syst Sci Data, 14: 2639-2679, https://doi.org/10.5194/essd-14-2639-2022, 2022.

Chen, W. On the export fluxes, seasonality and controls of particulate organic carbon in the Northern South China Sea. Xiamen University Xiamen, China, 2008.

Chen, Y.-l. L., Chen, H.-Y., Lin, Y.-H., Yong, T.-C., Taniuchi, Y., Tuo, S.-h.: The relative contributions of unicellular and filamentous diazotrophs to N_2 fixation in the South China Sea and the upstream Kuroshio. Deep-Sea Res Part I, 85: 56-71, https://doi.org/10.1016/j.dsr.2013.11.006, 2014.

Coale, K. H., Bruland, K. W.: Oceanic stratified euphotic zone as elucidated by ^{234}Th: ^{238}U disequilibria. Limnol Oceanogr, 32: 189-200, https://doi.org/10.4319/lo.1987.32.1.0189, 1987.

Cornec, M., Laxenaire, R., Speich, S., Claustre, H.: Impact of mesoscale eddies on deep chlorophyll maxima. Geophys Res Lett, 48: e2021GL093470, https://doi.org/10.1029/2021GL093470, 2021.

Dore, J. E., Karl, D. M.: Nitrite distributions and dynamics at Station ALOHA. Deep-Sea Res Part II, 43: 385-402, https://doi.org/10.1016/0967-0645(95)00105-0, 1996.

Du, C., He, R., Liu, Z., Huang, T., Wang, L., Yuan, Z., Xu, Y., Wang, Z., Dai, M.: Climatology of nutrient distributions in the South China Sea based on a large data set derived from a new algorithm. Prog Oceanogr, 195: 102586, https://doi.org/10.1016/j.pocean.2021.102586, 2021.

Du, C., Liu, Z., Dai, M., Kao, S.-J., Cao, Z., Zhang, Y., Huang, T., Wang, L., Li, Y.: Impact of the Kuroshio intrusion on the nutrient inventory in the upper northern South China Sea: insights from an isopycnal mixing model. Biogeosciences, 10: 6419-6432, https://doi.org/10.5194/bg-10-6419-2013, 2013.

Du, C., Liu, Z., Kao, S. J., Dai, M.: Diapycnal Fluxes of Nutrients in an Oligotrophic Oceanic Regime: The South China Sea. Geophys Res Lett, 44: 11,510-511,518, https://doi.org/10.1002/2017GL074921, 2017.

Eppley, R. W., Peterson, B. J.: Particulate organic matter flux and planktonic new production in the deep ocean. Nature, 282: 677-680, https://doi.org/10.1038/282677a0, 1979.

Estapa, M., Buesseler, K., Durkin, C. A., Omand, M., Benitez-Nelson, C. R., Roca-Martí, M., Breves, E., Kelly, R., Pike, S.: Biogenic sinking particle fluxes and sediment trap collection efficiency at Ocean Station Papa. Elementa: Science of the Anthropocene, 9: 00122, https://doi.org/10.1525/elementa.2020.00122, 2021.

Gan, J., Liu, Z., Liang, L.: Numerical modeling of intrinsically and extrinsically forced seasonal circulation in the China Seas: A kinematic study. J Geophys Res-Oceans, 121: 4697-4715, https://doi.org/10.1002/2016JC011800, 2016.

Gao, Y., Wang, L., Guo, X., Xu, Y., Luo, L.: Atmospheric wet and dry deposition of dissolved inorganic nitrogen to the South China Sea. Sci China: Earth Sci, 63: 1339-1352, https://doi.org/10.1007/s11430-019-9612-2, 2020.

Goldman, J. C.: Oceanic Nutrient Cycles. Springer US, https://doi.org/10.1007/978-1-4757-0387-0_6, 1984.

Gustafsson, Ö., Gelting, J., Andersson, P., Larsson, U., Roos, P.: An assessment of upper ocean carbon and nitrogen export fluxes on the boreal continental shelf: A 3-year study in the open Baltic Sea comparing sediment traps, ^{234}Th proxy, nutrient, and oxygen budgets. Limnol Oceanogr: Methods, 11: 495-510, https://doi.org/10.4319/lom.2013.11.495, 2013.

Haskell II, W. Z., Berelson, W. M., Hammond, D. E., Capone, D. G.: Particle sinking dynamics and POC fluxes in the Eastern Tropical South Pacific based on ^{234}Th budgets and sediment trap deployments. Deep-Sea Res Part I, 81: 1-13, https://doi.org/10.1016/j.dsr.2013.07.001, 2013.

He, Q., Zhan, H., Cai, S., Li, Z.: Eddy effects on surface chlorophyll in the northern South China Sea: Mechanism investigation and temporal variability analysis. Deep-Sea Res Part I, 112: 25-36, https://doi.org/10.1016/j.dsr.2016.03.004, 2016.

Hung, C. C., Gong, G. C.: Export flux of POC in the main stream of the Kuroshio. Geophys Res Lett, 34: L18606, https://doi.org/10.1029/2007GL030236, 2007.

Jiang, C., Cao, R., Lao, Q., Chen, F., Zhang, S., Bian, P.: Typhoon Merbok induced upwelling impact on material transport in the coastal northern South China Sea. PLoS One, 15: e0228220, https://doi.org/10.1371/journal.pone.0228220, 2020.

Johnson, K. S., Riser, S. C., Karl, D. M.: Nitrate supply from deep to near-surface waters of the North Pacific subtropical gyre. Nature, 465: 1062-1065, https://doi.org/10.1038/nature09170, 2010.

Kao, S. J., Terence Yang, J. Y., Liu, K. K., Dai, M., Chou, W. C., Lin, H. L., Ren, H.: Isotope constraints on particulate nitrogen source and dynamics in the upper water column of the oligotrophic South China Sea. Global Biogeochem Cycles, 26: GB2033, https://doi.org/10.1029/2011GB004091, 2012.

Kim, T. W., Lee, K., Duce, R., Liss, P.: Impact of atmospheric nitrogen deposition on phytoplankton productivity in the South China Sea. Geophys Res Lett, 41: 3156-3162, https://doi.org/10.1002/2014GL059665, 2014.

Knap, A., Michaels, A., Close, A., Ducklow, H., Dickson, A. J.: Protocols for the joint global ocean flux study (JGOFS) core measurements. Reprint of the IOC Manuals Guides No. 29, UNESCO, 19: https://doi.org/10.25607/OBP-1443, 1996.

Lampitt, R. S., Boorman, B., Lucas, M., L, Salter, I., Sanders, R., Saw, K., Seeyave, S., Thomalla, S. J., Turnewitsch, R.: Particle export from the euphotic zone: Estimates using a novel drifting sediment trap, ^{234}Th and new production. Deep-Sea Res Part I, 55: 1484-1502, https://doi.org/10.1016/j.dsr.2008.07.002, 2008.

Liu, K.-K., Kao, S.-J., Wen, L.-S., Chen, K.-L.: Carbon and nitrogen isotopic compositions of particulate organic matter and biogeochemical processes in the eutrophic Danshuei Estuary in northern Taiwan. Sci Total Environ, 382: 103-120, https://doi.org/10.1016/j.scitotenv.2007.04.019, 2007.

Liu, Y., Tang, D., Evgeny, M.: Chlorophyll concentration response to the typhoon wind-pump induced upper ocean processes considering air–sea heat exchange. Remote Sens, 11: 1825-1847, https://doi.org/10.3390/rs11151825, 2019.

Liu, Z., Zhao, Y., Colin, C., Stattegger, K., Wiesner, M. G., Huh, C.-A., Zhang, Y., Li, X., Sompongchaiyakul, P., You, C.-F., Huang, C.-Y., Liu, J. T., Siringan, F. P., Le, K. P., Sathiamurthy, E., Hantoro, W. S., Liu, J., Tuo, S., Zhao, S., Zhou, S., He, Z., Wang, Y., Bunsomboonsakul, S., Li, Y.: Source-to-sink transport processes of fluvial sediments in the South China Sea. Earth-Sci Rev, 153: 238-273, https://doi.org/10.1016/j.earscirev.2015.08.005, 2016.

Lu, Y., Wen, Z., Shi, D., Chen, M., Zhang, Y., Bonnet, S., Li, Y., Tian, J., Kao, S.-J.: Effect of light on N_2 fixation and net nitrogen release of *Trichodesmium* in a field study. Biogeosciences, 15: 1-12, https://doi.org/10.5194/bg-15-1-2018, 2018.

Ma, W. T., P. Xiu, F. Chai, L. H. Ran, M. G. Wiesner, J. Y. Xi, Y. W. Yan, and E. Fredj: Impact of mesoscale eddies on the source funnel of sediment trap measurements in the South China Sea, *Prog Oceanogr*, 194, https://doi.org/10.1016/j.pocean.2021.102566, 2021.

Mouriño-Carballido, B., Otero Ferrer, J. L., Fernández Castro, B., Marañón, E., Blazquez Maseda, M., Aguiar-González, B., Chouciño, P., Graña, R., Moreira-Coello, V., Villamaña, M.: Magnitude of nitrate turbulent diffusion in contrasting marine environments. Sci Rep, 11: 1-16, https://doi.org/10.1038/s41598-021-97731-4, 2021.

Okubo, A.: Oceanic diffusion diagrams. Deep-Sea Res, 18: 789-802, https://doi.org/10.1016/0011-7471(71)90046-5, 1971.

Owens, S. A., Buesseler, K. O., Sims, K.: Re-evaluating the ^{238}U-salinity relationship in seawater: Implications for the ^{238}U-^{234}Th disequilibrium method. Mar Chem, 127: 31-39, https://doi.org/10.1016/j.marchem.2011.07.005, 2011.

Puigcorbé, V., Masqué, P., Le Moigne, F. A.: Global database of oceanic particulate organic carbon to ^{234}Th ratios: Improving estimates of the biological carbon pump. Earth System Science Data, 12: 1267-1285, https://doi.org/10.5194/essd-12-1267-2020, 2020.

Resplandy, L., Martin, A. P., Le Moigne, F., Martin, P., Aquilina, A., Mémery, L., Lévy, M. and Sanders, R.: How does dynamical spatial variability impact ^{234}Th-derived estimates of organic export? Deep Sea Research Part I, 68: 24-45, https://doi.org/ 10.1016/j.dsr.2012.05.015, 2012.

Savoye, N., Benitez-Nelson, C., Burd, A. B., Cochran, J. K., Charette, M., Buesseler, K. O., Jackson, G. A., Roy-Barman, M., Schmidt, S., Elskens, M.: ^{234}Th sorption and export models in the water column: A review. Mar Chem, 100: 234-249, https://doi.org/10.1016/j.marchem.2005.10.014, 2006.

Scharek, R., Tupas, L. M., Karl, D. M.: Diatom fluxes to the deep sea in the oligotrophic North Pacific gyre at Station ALOHA. Mar Ecol-Prog Ser, 182: 55-67, https://doi.org/10.3354/meps182055, 1999.

Siegel, D. A., Buesseler, K. O., Behrenfeld, M. J., Benitez-Nelson, C. R., Emmanuel, B., Brzezinski, M. A., Adrian, B., Carlson, C. A., D'Asaro, E. A., Doney, S. C.: Prediction of the Export and Fate of Global Ocean Net Primary Production: The EXPORTS Science Plan. Fronti Mar Science, 3: 22, https://doi.org/10.3389/fmars.2016.00022, 2016.

Siegel, D. A., Cetinić, I., Graff, J. R., Lee, C. M., Nelson, N., Perry, M. J., Ramos, I. S., Steinberg, D. K., Buesseler, K., Hamme, R.: An operational overview of the EXport Processes in the Ocean from RemoTe Sensing (EXPORTS) Northeast Pacific field deployment. Elementa: Science of the Anthropocene, 9: 00107, https://doi.org/10.3389/fmars.2016.00022, 2021.

Stewart, G., Cochran, J., Miquel, J., Masqué, P., Szlosek, J., Baena, A. R., Fowler, S., Gasser, B., Hirschberg, D.: Comparing POC export from $^{234}Th/^{238}U$ and $^{210}Po/^{210}Pb$ disequilibria with estimates from sediment traps in the northwest Mediterranean. Deep-Sea Res Part I, 54: 1549-1570, https://doi.org/10.1016/j.dsr.2007.06.005, 2007.

Stukel, M. R., Kelly, T. B., Landry, M. R., Selph, K. E., Swalethorp, R.: Sinking carbon, nitrogen, and pigment flux within and beneath the euphotic zone in the oligotrophic, open-ocean Gulf of Mexico. J Plankton Res, https://doi.org/10.1093/plankt/fbab001, 2021.

Umhau, B. P., Benitez-Nelson, C. R., Close, H. G., Hannides, C. C., Motta, L., Popp, B. N., Blum, J. D., Drazen, J. C.: Seasonal and spatial changes in carbon and nitrogen fluxes estimated using ^{234}Th: ^{238}U disequilibria in the North Pacific tropical and subtropical gyre. Mar Chem, 217: 103705, https://doi.org/10.1016/j.marchem.2019.103705, 2019.

Wang, L., B. Q. Huang, E. A. Laws, K. B. Zhou, X. Liu, Y. Y. Xie, and M. H. Dai: Anticyclonic Eddy Edge Effects on Phytoplankton Communities and Particle Export in the Northern South China Sea, *J Geophys Res-Oceans*, 123, 7632-7650, https://doi.org/10.1029/2017jc013623, 2018.

Winn, C. D., Campbell, L., Christian, J. R., Letelier, R. M., Hebel, D. V., Dore, J. E., Fujieki, L., Karl, D. M.: Seasonal variability in the phytoplankton community of the North Pacific Subtropical Gyre. Global Biogeochem Cycles, 9: 605-620, https://doi.org/10.1029/95GB02149, 1995.

Wu, J., Lee, Z., Xie, Y., Goes, J., Huang, B.: Reconciling between optical and Biological determinants of the euphotic zone depth. J Geophys Res-Oceans, 126: e2020JC016874, https://doi.org/10.1029/2020JC016874, 2021.

Xie, Y., Laws, E. A., Yang, L., Huang, B.: Diel patterns of variable fluorescence and carbon fixation of picocyanobacteria *Prochlorococcus*-dominated phytoplankton in the South China Sea basin. Front in Microbiol, 9: 1589-1604, https://doi.org/10.3389/fmicb.2018.01589, 2018.

Yang, J.-Y., Hsu, S.-C., Dai, M., Hsiao, S.-Y., Kao, S.-J.: Isotopic composition of water-soluble nitrate in bulk atmospheric deposition at Dongsha Island: sources and implications of external N supply to the northern South China Sea. Biogeosciences, 11: 1833-1846, https://doi.org/10.5194/bg-11-1833-2014, 2014.

Yang, J. Y. T., Kao, S. J., Dai, M., Yan, X., Lin, H. L.: Examining N cycling in the northern South China Sea from N isotopic signals in nitrate and particulate phases. J Geophys Res-Biogeoscience, 122: 2118-2136, https://doi.org/10.1002/2016JG003618, 2017.

Yang, J. Y. T., Tang, J. M., Kang, S., Dai, M., Kao, S. J., Yan, X., Xu, M. N., Du, C.: Comparison of nitrate isotopes between the South China Sea and western North Pacific Ocean: Insights into biogeochemical signals and water exchange. J Geophys Res-Oceans, 127: e2021JC018304, https://doi.org/10.1029/2021JC018304, 2022.

Zhou, K., Dai, M., Kao, S.-J., Wang, L., Xiu, P., Chai, F., Tian, J., Liu, Y.: Apparent enhancement of ^{234}Th-based particle export associated with anticyclonic eddies. Earth Planetary Science Letters, 381: 198-209, https://doi.org/10.1016/j.epsl.2013.07.039, 2013.

Zhou, K., Dai, M., Maiti, K., Chen, W., Xie, Y.: Impact of physical and biogeochemical forcing on particle export in the South China Sea. Progress In Oceanography, 187: 102403, https://doi.org/10.1016/j.pocean.2020.102403, 2020a.

Zhou, K., Dai, M., Xiu, P., Wang, L., Hu, J., Benitez-Nelson, C. R.: Transient enhancement and decoupling of carbon and opal export in cyclonic eddies. J Geophys Res-Oceans, 125: e2020JC016372, https://doi.org/10.1029/2020JC016372, 2020b.